Characterization of Turbine Rim Seal Flow and its Sealing Effectiveness

by

Peter T. Catalfamo

B.S. Aeronautical and Mechanical Engineering
Rensselaer Polytechnic Institute (2008)

Submitted to the Department of Aeronautics and Astronautics
in partial fulfillment of the requirements for the degree of

Master of Science in Aeronautics and Astronautics

at the

MASSACHUSETTS INSTITUTE OF TECHNOLOGY

June 2013

Author .....
Department of Aeronautics and Astronautics
May 23, 2013

Certified by .....
Choon S. Tan
Senior Research Engineer of Aeronautics and Astronautics
Thesis Supervisor

Accepted by .....
Eytan H. Modiano
Professor of Aeronautics and Astronautics
Chair, Graduate Program Committee

Characterization of Turbine Rim Seal Flow and its Sealing Effectiveness

by

Peter T. Catalfamo

Submitted to the Department of Aeronautics and Astronautics
on May 23, 2013, in partial fulfillment of the
requirements for the degree of
Master of Science in Aeronautics and Astronautics

Abstract

In a gas turbine engine, ingestion of hot gas from the flowpath into the gaps between the turbine rotor and stator can lead to elevated metal temperatures and a deterioration of component life. To prevent ingestion, bleed air from the compressor is used to "purge" the rim seal cavities. Establishing a quantitative understanding of the wheelspace and rim cavity flow processes driving ingestion is critical to optimizing seal design and minimizing the associated performance penalty. A computational model of the wheelspace that does not limit the spatial or temporal scales of flow processes is formulated. This allows the assessment of the response of the wheelspace to external stimuli set up by the turbine main flow path, and the development of causal links between flow processes and their drivers. Varying the axisymmetric turbine flowpath pressure on a quasi-steady basis when the purge flow supply seal is choked has no impact on ingestion; the pressure field in the wheelspace merely scales with the flowpath pressure, leaving the flow structure unchanged. Introducing circumferential variation in the external pressure field can, however, lead to ingestion with the ratio of disturbance wavelength to the trench depth emerging as a key parameter. Varying rotational speed alone does not drive ingestion as a stagnation point is formed on the outer shroud that is ingestion resistant. It is shown that excitation at frequencies corresponding to the natural modes of the wheelspace system can lead to large responses in pressure and seal flow rate, with the seal reduced frequency appearing as a characterizing parameter. The existence and parametric dependence of these modes is further assessed through a small disturbance flow analysis. A generalized small disturbance flow analysis is formulated that provides a direct enumeration of the key characterizing parameters.

Thesis Supervisor: Choon S. Tan
Title: Senior Research Engineer of Aeronautics and Astronautics

Acknowledgments

The work presented here would not have been possible without the support and guidance of a great number of people, among them teachers, colleagues, family, and friends. I am deeply grateful for their help and would like to use this opportunity to recognize them.

First I would like to thank my advisor, Dr. Choon Tan. His encouragement and guidance has been invaluable to the progress of this research. His frequent advice and good-humored encouragement to think outside of the box has forced me to greatly expand my base of knowledge and change the way I think. He consistently urged me to avoid over-constraining my thoughts, a valuable lesson that I hope to continue to improve upon. I greatly look forward to even more such learning and growth through continued work with him. He has truly been a great teacher.

I have also benefitted greatly from the input of my colleagues at General Electric. The program sponsors, Dr. Kevin Kirtley and Ben Ding of G.E. Power and Water have monitored progress and given suggestions and encouragement throughout the process. Their insight and experience ensured the steady progress of this research in what is hopefully a beneficial direction. Dr. Pepe Palafox of G.E. Global Research whose experience in the area, especially regarding wheelspace experiments, has made him another great resource.

I would like to extend special thanks to Dr. Greg Laskowski of G.E. Aviation who has, through numerous formal and informal discussions guided me greatly throughout the course of the research. His great wealth of knowledge on the mechanics of CFD modeling, especially regarding wheelspace modeling, has been an amazing resource. His consistent support and encouragement throughout has been the source of much inspiration and cannot be overstated.

I would also like to greatly thank the leadership of the Aviation thermal systems design organization, Tim Stone of G.E. Aviation, Beth Schumacher of G.E. Aviation, and my immediate manager Jordan Schwartz also of G.E. Aviation for their continued support throughout. Having representatives of both the industrial and avi-

ation sectors has highlighted the importance of this research across a great range of applications.

Many thanks to General Electric for sponsoring and funding this research through a research contract with MIT and for supporting my studies through its Advanced Courses in Engineering program.

Lastly I would like to thank my family who have supported me in everything from the beginning. My parents have always encouraged me to grow intellectually and have been a source of constant support throughout my education. A special thanks to my wife, Kelly, who has quietly put up with many long nights in the GTL, and continues to encourage me despite this.

Contents

List of Figures

List of Tables

Nomenclature

Non-Dimensional Characterizing Parameters

$\mathcal{AR}$	Wheelspace aspect ratio
ΔC_p	Flowpath disturbance pressure coefficient
Φ	Turbine stage loading coefficient
C_w	Non-dimensional cooling mass flow
G_c	Seal clearance ratio
Re_w	Reynold's number in main flowpath
Re_ϕ	Rotational Reynold's number
Re_{seal}	Reynold's number in seal
Ro	Rossby Number

Subscripts and Superscripts

$*$	Non-Dimensionalized
$'$	Indicates Disturbance Quantity
e	Exit
i	Ingested
in	Inlet

p	Purge
$\bar{}$	Indicates Mean Flow

Variables

Ω	Angular Velocity
ω	Disturbance Frequency
ρ	Density
a	Speed of Sound
b	Rim Radius
c_p	Specific Heat at Constant Pressure
k	Circumferential Wave Number
L_t	Seal Thickness
n	Radial Wave Number
N_b	Number of Blades
N_v	Number of Vanes
p	Pressure
s	Specific Entropy
T	Temperature
u	Radial Velocity
U	Characteristic Radial Velocity
V	Characteristic Tangential Velocity
v	Tangential Velocity
w	Axial Velocity

Chapter 1

Introduction

Gas turbine engines have become an ubiquitous technology, having uses in a great number of applications including power generation, land and marine transportation, and aviation propulsion. Natural gas plants (i.e. gas turbines) will make up nearly 75% of the increase in net capacity of new power plants to be built between 2012 and 2016, according to a report compiled by the US Energy Information Agency [1]. In nearly every application of gas turbines, from industrial power generation to aircraft engines, fuel cost is a major driver of operator profit margins and therefore fuel economy of the generator (or engine) is a critical metric. Rising fuel prices and growing environmental concerns have only made efficiency more important.

To achieve these ever higher efficiency goals the turbine inlet temperature has steadily risen over the past several decades such that modern turbines operate well above the melting point of available metal alloys. The flowpath components that see this temperature directly are typically made of exotic alloys capable of withstanding high temperatures (well beyond their melting point) and incorporate advanced cooling technologies (e.g., convective and film cooling and thermal barrier coatings). Those components outside of the flowpath (e.g., rotor disks and structural components), however, are not capable of tolerating these elevated temperatures. Due to the requirement that one part be rotating and one stationary, there are by necessity gaps in the flowpath to allow relative motion. Ingress of the hot flowpath air through these gaps into the wheelspace cavity can lead to rapid deterioration of these less

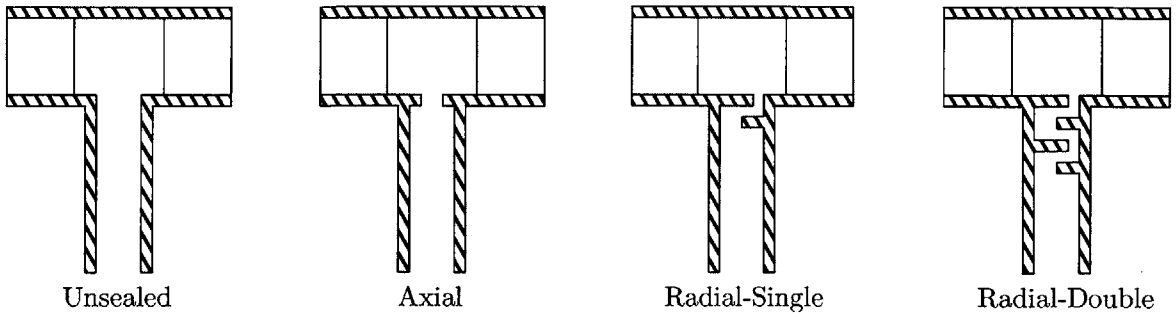

Figure 1-1: *Illustration of canonical rim seal configurations. Shown from left to right, unsealed wheelspace, a simple axial seal, seal with a single radial clearance, and a seal with two radial clearances. These represent the typical configurations found in gas turbine applications*

capable parts' lives and premature failure.

To prevent this, "cool" air is bled off of the late stages of the compressor and used to pressurize the cavities between the rotor and stator and "purge" the gaps in the flowpath. Seals upstream of the wheelspace are used to control the amount of air supplied for purging the flowpath gaps.

The use of this purge flow, however, negatively impacts cycle efficiency. Work is done compressing the air in the compressor but, since the air does not pass through the combustor and is not properly turned prior to entering the rotor row, less work can be extracted from it. There are also mixing losses associated with the reintroduction of the air into the flowpath, which negatively impacts turbine efficiency[14]. Therefore, in the drive to improve efficiency there is a strong desire to reduce the purge flow necessary to prevent adverse impacts due to ingestion. The amount of purge flow required to prevent ingestion has been found to strongly depend on the configuration of the rim seal (the interface between rotor and stator hubs). Fig. 1-1 shows illustrations of several commonly used rim seal geometries. Studies have shown that radial seals tend to be more effective than axial seals.

The goal of this research is to identify the flow processes driving ingestion and limiting sealing effectiveness.

1.1 Literature Review

Flow in gas turbine wheelspace cavities has been an active area of research dating back to the early days of the jet age. Notably in the 1950s, Batchelor and Stewartson published seminal papers on the structure of flow in rotor stator cavities in different regimes. Batchelor contended that any radial flow is confined to the boundary layers on the rotor stator surface and that the system is characterized by an inviscid core in solid body rotation [2]. Stewartson argued that there was no such core and that the flow more gradually transitioned between rotor and stator [13]. Experiments have since shown both Batchelor and Stewartson were correct, with the flow approximating Stewartson behavior at low rotational speed and Batchelor type flow at higher speeds. Daily and Nece [3] categorized the wheelspace cavity flow regimes as function of rotational Reynolds number and rotor-stator spacing.

Since these foundational findings on rotor-stator wheelspace flow, the gas turbine industry has placed much focus on finding an optimal sealing configuration. A great number of experimental studies have been performed by Owen et. al [9][10][11][12], leading to a number of papers with a focus on developing orifice-type models. While these models have found use in direct design applications, they are limited in their generality by the geometry and configurations tested.

More recently, in the past decade or two, increasing attention has been given to computational studies of turbine rim cavity flow, such as those performed by Jakoby [6], Laskowski [8], Hills [5], and others. These studies have largely consisted of sector models of engine geometry, including the flowpath components. While this type of computational model has usefulness in showing the detailed flow field in true-to-product configurations, its utility for elucidating the drivers of key flow features is limited. The primary difficulty arising from these complex models is the challenge of assigning cause and effect to the emergence of flow features or phenomena. Because of their complexity, there are numerous effects induced by the main turbine and wheelspace flowpaths that impact ingestion; separating these out and distinguishing what specific design feature is driving it is difficult. Furthermore, the sector model

Table 1.1: Table of Characteristic Parameters and Typical Ranges based on review of published literature

Parameter	Typical Range
Re_ϕ	$1 \times 10^5 - 5 \times 10^7$
ΔC_p	0.05-0.8
C_w	0-20000
G_c	0.01-0.05
$\mathcal{R}$	0.05-0.1

excludes flow features with length scale larger than the sector.

Through these previous research efforts several characterizing parameters, both geometric and fluid dynamic, have been identified and explored. Table 1.1 provides a brief overview of these parameters and the typical ranges reported in the literature. These parameters include the rotational Reynolds number, the non-dimensional purge flow rate, and several geometric characterizations.

1.2 Objectives

This research seeks to build on this body of work and expand the knowledge of the key drivers of ingestion and characterizing parameters in a form that can be applied generally. A review of the problem and existing literature leads to several overarching research questions.

1. What role do rim cavity modes and flow unsteadiness play?
2. What drivers limit the sealing effectiveness of rim seals?
3. What are the required attributes of CFD to adequately capture ingestion phenomena?
4. What are the sources of loss, and how are they linked to sealing effectiveness?
5. What sets the acceptable ingestion level before adversely impacting part life or durability?

This thesis does not attempt to address all of these questions but recognizes them as the final goal. The research described in this thesis focuses on the top two questions regarding the drivers of sealing effectiveness and the role of resonance (i.e. Excitation of the wheelspace cavity modes) and flow unsteadiness.

1.3 Contributions and Findings

A computational model for turbine annular wheelspace flow is formulated. The model allows for the analysis of wheelspace flow behavior in response to the pressure field in the turbine main flowpath. This pressure field is set by the turbine nozzle guide vane and rotor stage design. This assumption that the turbine flowpath pressure field is essentially independent of the wheelspace makes it computationally tractable to model the full 360° wheelspace. As such the model does not restrict the spatial or temporal scales of the induced flow processes in the cavity as a sector model does. Furthermore the model enables the establishment of specific cause-and-effect. Specifically, the computational model has been used to elucidate the following findings:

1. The assumption of constant (choked) supply flow has implications for the quasi-steady response of the wheelspace flow structure. With the inlet flow choked variations in the absolute level of the downstream pressure cause the wheelspace pressure field to scale up or down, but the flow structure and amount of purge flow remains the same. Because of this, quasi-steady variations in the axisymmetric pressure field do not lead to ingestion while the seal remains choked.

2. Circumferential variation in the external pressure field can lead to ingestion. This was assessed by imposing a periodic variation around the circumference of the rim. These studies identified the ratio of disturbance wavelength to trench depth as an important characterizing parameter.

3. Over a range of rotational Reynolds numbers of interest in gas turbines ingestion could not be driven for a steady axisymmetric turbine flow path pressure field by varying rotational speed alone. A key feature preventing ingestion is the

formation of a stagnation point on the shroud. The flow that is pumped up the rotor boundary layer and impinges on the outer shroud thus generating a local high pressure zone at the seal that resists ingestion.

4. Varying the purge flow rate, with an axisymmetric external pressure field, did not lead to the onset of ingestion. As was shown in the case of varying rotational speed, it appears there needs to be another driver, such as a non-axisymmetric external pressure field, to drive ingestion on a quasi-steady basis.

5. Unsteadiness and, in particular, resonance (the excitation of cavity modes) could have a significant impact on sealing effectiveness. An unsteady axisymmetric pressure field in the turbine main flow path induces strong responses in both pressure and seal mass flow rate when frequencies corresponding to those of the natural cavity modes are imposed in the turbine main flowpath. It also suggests that the seal reduced frequency, defined as $\frac{\omega L_t}{U_{seal}}$ the ratio of the characteristic convection time through the seal to the unsteady timescale, is a characterizing parameter for ingestion. The influence of resonance on rim cavity sealing has not to this author's knowledge been addressed in the publicly available literature. Characterizing the natural modes of the system is an important step towards understanding an aspect of ingestion response.

6. An unsteady non-axisymmetric pressure field in the turbine main flow path, similar to the steady circumferential variation, can lead to ingestion. In this case, however, the ratio between the phase speed of the pressure field and the swirl in the wheelspace is an important parameter. This has been discussed in the literature and was confirmed in these studies.

A generalized small disturbance analysis of turbine wheelspace flow has been formulated for direct determination of eigen frequencies and associated eigen modes. The analysis also provides an alternative means to assess the unsteady non-axisymmetric flow disturbances in the wheelspace with a characteristic mean flow (radial swirling throughflow and temperature non-uniformity) in response to the pressure imposed by

the turbine flow path. We inferred from the analysis the following non-dimensional characterizing parameters for the cavity modes:

1. The rim mach number: $\frac{\Omega b}{\bar{a}}$
2. The ratio of characteristic radial throughflow velocity to the characteristic tangential velocity: $\frac{U}{V}$.
3. The ratio of tangential velocity to rim speed: $\frac{V}{\Omega b}$
4. The ratio of radial throughflow velocity to rim speed: $\frac{U}{\Omega b}$
5. The product of the tangential and radial throughflow Mach numbers: $\frac{UV}{\bar{a}^2}$
6. The non-dimensional mean radius of the wheelspace: $\frac{R_m}{b}$
7. The compactness ratio based on the disturbance frequency: $\frac{\omega b}{\bar{a}}$
8. The ratio of the disturbance phase speed to the disk rotating speed: $\frac{\omega}{k\Omega}$

These parameters come directly from the non-dimensionalization but it should be noted that they are not all independent (e.g. items 3 and 4 can be combined to yield 2).

For the situation of simple wheelspace flow consisting of no mean flow with non-rotating discs, the analysis shows the existence of a three-harmonic circumferential rotating modes in accord with experimental measurements. The addition of rotation also shows the existence of these modes, but with higher frequencies corresponding to a stiffening of the system.

1.4 Thesis Organization

In chapter 2, an overview of the research approach is presented. This chapter attempts to lay out the thought process and reasoning behind the methodology chosen for

answering the research questions. A brief outline of each of the major aspects of the approach taken is given.

Chapter 3 describes the computational modeling. This expands on the basic approach detailed in chapter 2 and gives a detailed description of the modeling and results. Similarly chapter 4 details the small disturbance analysis carried out and results to date. Chapters 5 and 6 summarize the findings and detail future work to continue the research initiated in this thesis.

Chapter 2

Research Approach

As was described in section 1.1, previous research efforts have primarily focused on developing correlative models that can be used directly in the design of turbine rim seals. This largely involved running tests on various configurations and developing empirical models to describe when ingestion would occur in that configuration. This approach leaves much of the design space unexplored however and the models derived from them is limited in its applicability to the configurations tested. The effort described here seeks to avoid this lack of generality by linking flow features to the specific physical events driving them. The goal of this is to identify the non-dimensional parameters that control the sealing effectiveness of a canonical seal configuration. Two complementary approaches were taken. A series of computational simulations (using the commercial package CFX) of increasing level of physical complexity were undertaken to establish parametric trends and to develop links between effect (e.g. ingestion) and cause (e.g. a specific flow feature). This is described in section 2.1. Along with these CFD studies, a small disturbance flow analysis was used to develop an analytical tool for identifying the natural modes of a canonical wheelspace cavity. This modal analysis is described in section 2.2.

2.1 Incremental Modeling

The wheelspace and rim cavity constitutes a rich aero-thermal environment with complex geometric features. In a model that includes all of this complexity it can be difficult to assign with any rigor the emergence of a flow phenomenon to any one driver. In order to disentangle these drivers and be able to assign causal relationships an incremental approach was adopted. In starting with an extremely simple geometry, with simple boundary conditions, and adding complexity on an incremental basis we can see the incremental effect each addition has on the flow field and sealing effectiveness. Fig. 2-1 shows the simplified wheelspace configuration and dimensional nomenclature that will be used throughout this thesis.

One key differentiating feature of the approach taken here to previous numerical analyses is the treatment of the flowpath. The purge flow for a given rotor-stator cavity is typically on the order of 1% of the flow in the main gas path [8][7]. As a result, the pressure field in the main flow path can be assumed to be fairly insensitive to the details of the rim seal cavity and purge flow itself. This has large implications for modeling. If the main flowpath pressure field can be approximated as insensitive to the details of the purge flow cavity, the two problems can be decoupled. This is the approach taken here, it is assumed that the main flowpath pressure field is essentially set by the design of the flowpath hardware (turbine/nozzle aerodynamics). This fixed pressure field can now be directly used as a boundary condition for the wheelspace flow model.

In eliminating the need to compute the flow through the main flowpath, a great amount of computational resources have been freed up. All of the resources that were previously dedicated to blade/nozzle/flowpath modeling can now be allocated to assessing the wheelspace aerothermal flow physics.. Previous modeling efforts, because they almost universally include explicit modeling of the flowpath, have been limited to small sector models. While a sector model is computationally efficient it has the downside of restricting the periodicity of modes that can be modeled. Modes of longer wavelength than the sector, such as the low order modes which some

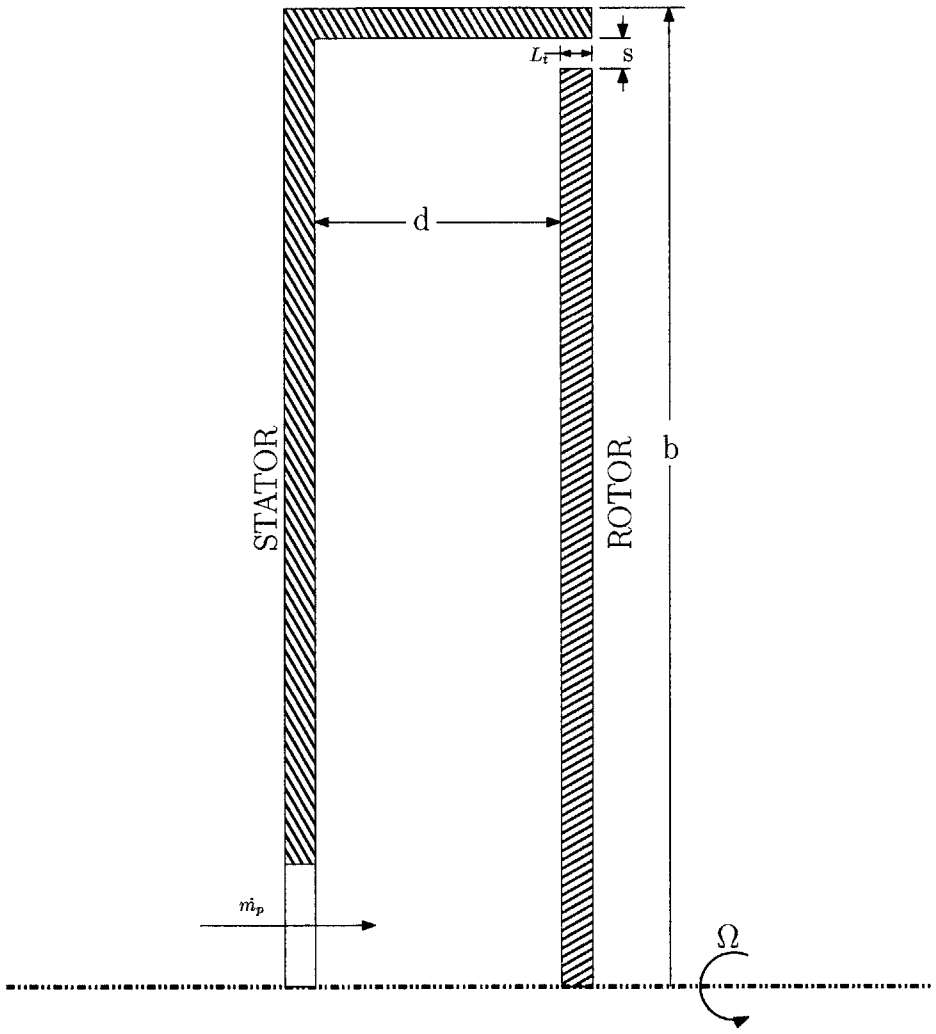

Figure 2-1: *Illustration of canonical wheelspace configuration and nomenclature.*

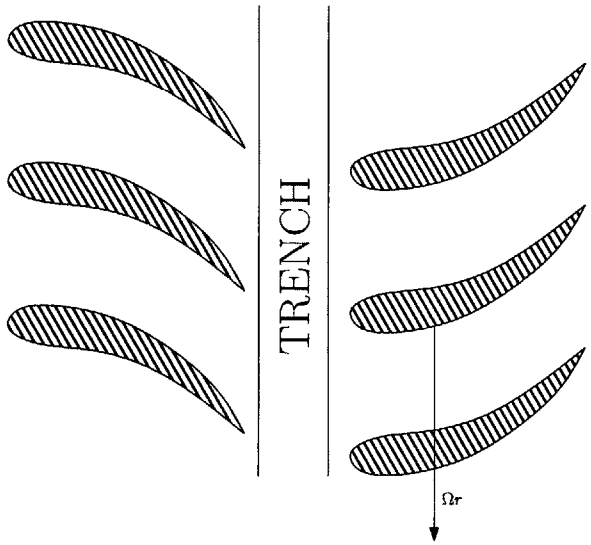

Figure 2-2: *Illustration showing trench cavity in relation to rotor and turbomachinery components.*

experiments have shown to exist [6], may be important, or modes that do not match the periodicity of the sector can be suppressed. The elimination of the flowpath allows for a full 360° model without prohibitive computational cost.

Further, the flowpath boundary condition can be decomposed into a superposition of harmonic modes generated by the various flowpath components as shown in equation 2.1.

$$p(r,\theta,x,t) = \sum_{n=-\infty}^{\infty} \sum_{k=-\infty}^{\infty} Q(r,x)\, e^{inN_b\Omega t - i(kN_v + nN_b)\theta} \tag{2.1}$$

While what is shown in equation 2.1 includes only the effects of the blade and nozzle rows depicted in Fig. 2-2, this framework can be extended to include any periodic pressure field, such as that generated by the shedding wakes off of the nozzle, any lower frequency modes such as that caused by casing out of round. This approach fits naturally with the overall research approach of incremental assessment. By reducing the flowpath pressure field to a superposition of harmonics, we can assess each contributing factor one by one, building them on top of each other until we reach a pressure field representative of the engine configuration.

2.2 Modal Analysis

One of the primary goals of this research is to identify the role of resonance in wheelspace cavity flows and its importance in ingestion. To do this a detailed characterization of the response to stimuli must be developed. While this could be accomplished through extensive computational modeling. A simpler direct method for determining the natural frequencies and modes of canonical wheelspace configurations is desired.

To accomplish this a small disturbance flow analysis was carried out to generate a tool capable of identifying the natural modes and frequencies. There are a number of advantages to this approach. First, computational studies can be costly to run in both time and resources and are cumbersome for effective parametric studies. The simplicity of the small disturbance model on the other hand allows it to be useful for effective parametric assessments.

Along with this, the analytical formulation allows the key controlling parameters to become immediately obvious in the equations themselves. Finding these parameters through computational studies alone would not be as direct. The form of the resulting equations generated can also give insight into the impact of these parameters on the flow physics, something which would be difficult with computational studies alone.

The basic approach consists of developing the equations of motion for a characteristic system, linearizing these, and then solving the resulting eigenvalue problem. This is detailed in chapter 4.

2.3 Summary of Research Approach

The approach taken to begin addressing the research questions posed in chapter 1 is based on computational analysis of incremental levels of physical complexity that is representative of turbine wheelspace cavity flow. A computational model is used to map out the parametric dependencies governing ingestion. Through progressive

implementation of complexity into the model, causal relationships can be established. The computational model is complemented by an analytical small disturbance model for determining the natural frequencies and mode shapes of a canonical wheelspace geometry as well as for directly establishing ingestion criteria.

Chapter 3

Computational Analysis

The rapid advancement of computing technology in the past decade has made detailed unsteady computational modeling an increasingly useful research tool. Described here is the development of a 3-D computational model of a canonical wheelspace and rim cavity seal using the commercial CFD software ANSYS CFX version 14.5.

3.1 Methodology and Setup

The wheelspace/rim cavity system is a complex system of seals and interrupted cavity geometries containing swirling radial outflow with potentially large rim-bore gradients; as such the resulting aero-thermal environment provides a fertile ground for flow phenomena. In order to model the system efficiently in a way that can tractably be understood it must be reduced to a simpler system. To accomplish this, the wheelspace cavity is represented as a simple smooth walled rotor/stator system with a constant axial gap. A canonical radial seal geometry typical of industrial gas turbines was used. A representative computational domain can be seen in figure 3-1.

In a gas turbine, amount of purge flow supplied is controlled by a seal or series of seals that meter the amount of air bled off of the compressor. These seals are often, though not always at or near choked conditions. To translate this into the computational model, the inlet boundary condition was set as a stagnation pressure (this pressure is essentially fixed by the design of the compressor and the bleed location) at

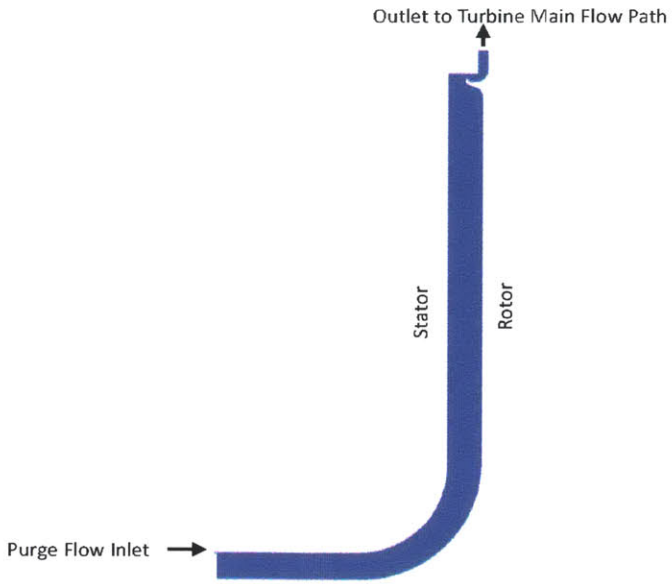

Figure 3-1: *Computational domain*

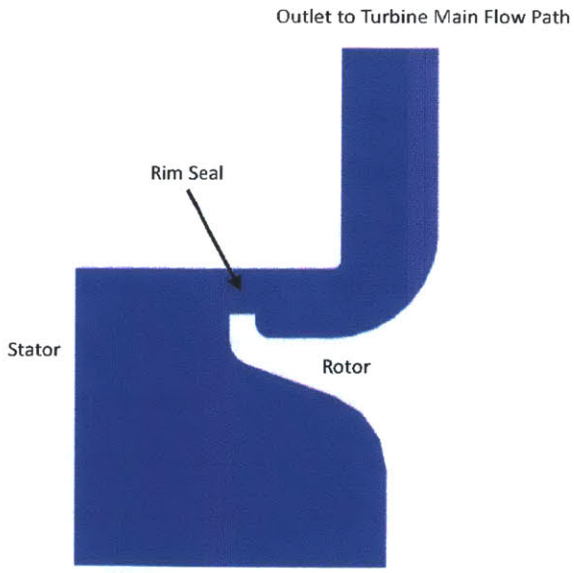

Figure 3-2: *Close up of the rim seal geometry modeled as a canonical radial seal.*

the inlet with a restriction (i.e. a throttle) to meter the flow. In many of the numerical studies in literature the inlet boundary condition is set as a fixed mass flow to give direct control over the amount of purge flow. While this is convenient it is limited by not allowing the flow rate to respond to changes in the cavity. The stagnation pressure/restriction area boundary provides a much more physical condition at the inlet which allows the steady and unsteady response of the supplied purge flow rate to react to pressure field changes within the cavity.

The outlet boundary condition is specified as an opening condition with a specified static pressure field along the wheel space flow exit slot. The opening is used in place of an outlet boundary due to the presence of combined inflow/outflow at the boundary. In the analyses shown here any inflow is assumed to enter normal to the outlet (i.e. purely radially). This simplifies the formulation of the boundary condition but does leave out the potentially important impact of ingested swirl from the main flowpath. As one of the goals of the research was to assess the flow response to different imposed pressure fields this simplification was deemed justifiable on a physical basis. This is an assumption that needs to be further addressed in future work.

The rotor and stator surface boundary conditions are defined as smooth, adiabatic walls with the rotor surface rotating at a specified speed.

The success of any flow computation is largely dependent on the quality of the mesh used. A baseline structured mesh consisting of approximately 3 million cells was created using Pointwise version 17. This mesh was designed to provide maximum resolution near the rim seal which is the primary area of interest and also the location where the most complex phenomenon are expected. Figure 3-3 shows the mesh in the region of the rim seal.

The boundary layer resolution was designed to be sufficient for a wall-function approach with y^+ values of $10 - 30$. The steady simulations were run until RMS residuals converged to less than 1×10^{-6}. A grid sensitivity study was performed using a mesh of 1.5 times the grid density, and one with half the grid density. This study was performed on the baseline steady simulation and the resulting pressure fields were compared. A contour plot of the normalized difference in pressure between

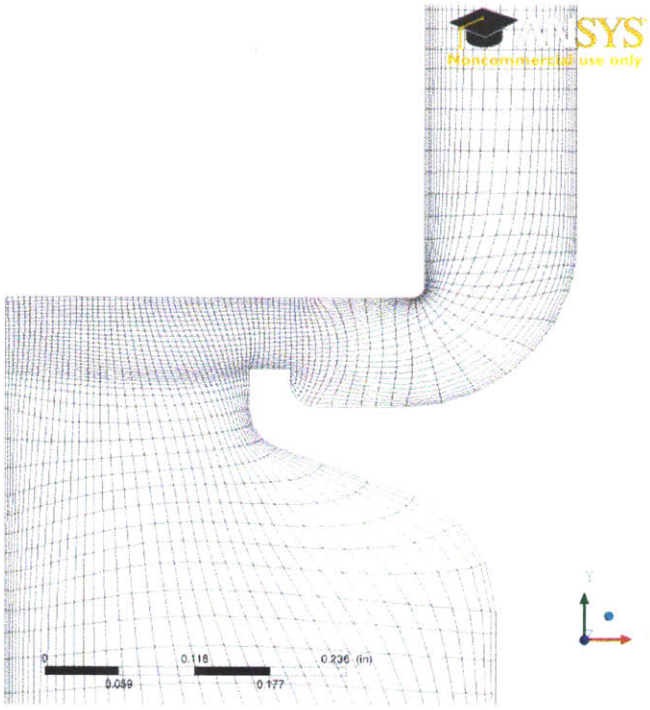

Figure 3-3: *Mesh in the rim seal region*

the baseline grid resolution and the fine grid resolution are shown in figure 3-4. This clearly shows that between the baseline grid and the fine grid the pressure field is unchanged over the vast bulk of the domain with only minor differences in regions of high gradients. Based on this the baseline grid was determined to provide sufficient resolution for the purposes of this analysis.

As the focus is on unsteady and resonant response, a number of transient simulations were performed. To ensure the accuracy of the unsteady simulations the timestep was selected for each case to reach convergence within 2-5 coefficient loop iterations, and chosen such that the RMS Courant number was approximately equal to 1. The transient simulations were run using converged steady solutions as initial conditions. Simulations were continued until the transients resulting from the initial conditions had diminished to a negligible level. This was confirmed through monitoring test points measuring the pressure field upstream and downstream of the seal, as well as the mass flow rate through the seal.

Using this setup a number of studies were performed to assess the impact of the

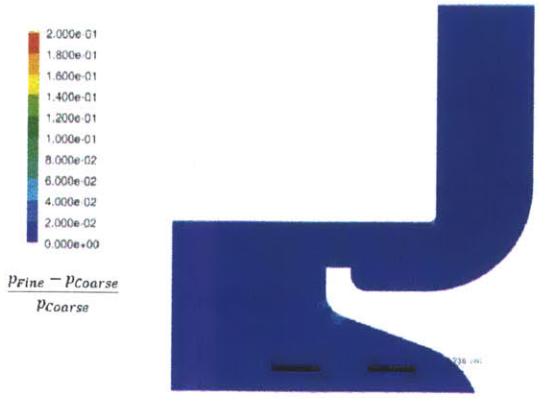

Figure 3-4: *Results of the grid sensitivity study. Contours of the percent difference in pressure between the fine and coarse grid. The peak differences occur in regions of rapid transition (sharp corners etc.) where pressure gradients are expected to be high. Maximum difference is less than .1%.*

outlet boundary conditions, rotational speed, and select geometrical features on the flow field within the cavity. These studies and their results are described in the following section.

3.2 Results

The following sections discuss the results of a series of assessments on the impact of various design variables on ingestion. The basic flow is in line with the overall research approach, each variable is assessed individually and complexity in the boundary conditions is added incrementally. We begin with assessments of the impact of design variables such as rotor speed, purge mass flow, and seal configuration subject to a steady axisymmetric turbine main path pressure field. This provides for the assessment of the influence of these parameters alone on ingestion. The turbine main flow path pressure field is then assumed to be circumferentially periodic, but still steady, representative of an NGV row and the impact on ingestion is assessed. This approach is continued with the assessment of the impact of a rotating, circumferentially periodic, boundary condition representative of a blade row. The results of these studies

is described in the following.

3.2.1 Steady Axisymmetric

The studies described in this section were performed using a steady, uniform axisymmetric pressure distribution at the outlet (i.e. no axial or circumferential variation). The results contained here are from steady state analyses. The goal of these studies was to assess the parametric impact of rotational speed and outlet pressure level on the wheelspace pressure/flow field and its ingestion characteristics.

Rotational Speed Parametric Study

In this study the rotational Reynolds number was varied from $Re_\phi = 0$ to $Re_\phi = 1 \times 10^7$ by varying the rotational speed of the rotor. All other boundary conditions and the geometry remain fixed. The non-dimensional mass flow supply was $C_w = 7250$, which represents a typical intermediate flow rate corresponding to 0.8% of core flow for the configuration examined.

Contour plots of the pressure field with streamlines superimposed at three rotational speeds are shown in figures 3-5 through 3-7. From this analysis it was shown that over a range of rotational Reynolds number of interest in gas turbines, ingestion could not be driven under these conditions by varying rotational speed alone. A key feature preventing such ingestion is the formation of a radial stagnation point on the shroud. This results from the impingement of the flow that is pumped up along the rotor onto the shroud, the radial outflow splits at this stagnation point, with a portion of the flow turning aft and going out through the seal, and a portion turning forward and returning as radial inflow along the stator surface. As a result of this stagnation point there is a high pressure zone right at the seal that prevents ingestion. As long as the stagnation point exists and there is a non-zero purge flow entering the wheelspace system ingestion is not possible on a steady basis by continuity.

As the rotational speed is increased, the stagnation point tends to move aft towards the seal. If the flow coming off the rotor were to be fully turned such that it did not

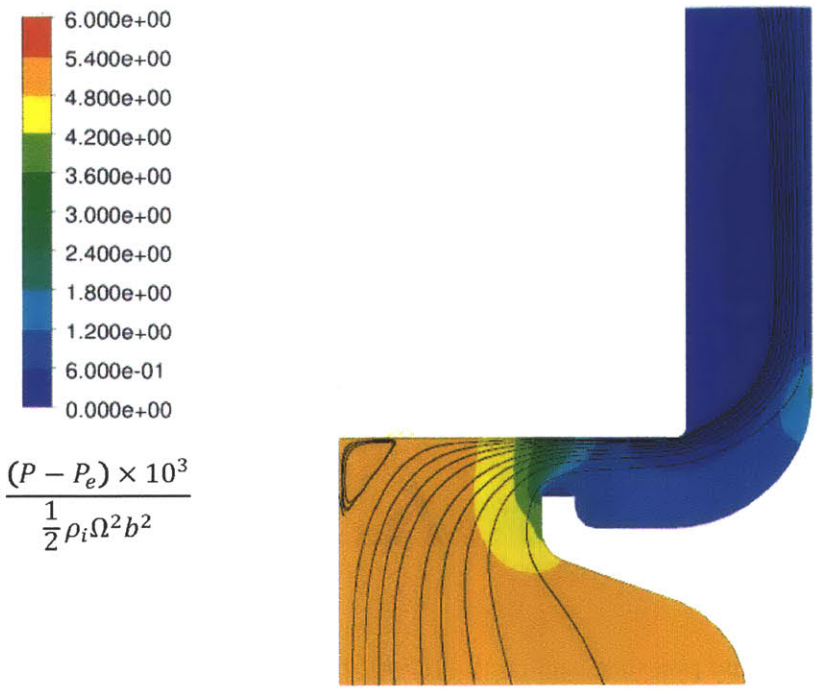

Figure 3-5: *Streamlines and pressure field contours for $Re_\Phi = 0$. There is no rotation, and no stagnation point in the seal region can be seen.*

impinge on the shroud surface it would enable ingestion to occur along the top surface. This was not observed in any of the computations to date. The radius of curvature of the streamlines coming off the rotor is set by the ratio of the fluid inertia (i.e. pumping velocity due to rotor) to the pressure drop across the seal. If the resulting radius of curvature is greater than the clearance there would be no stagnation point and one could infer an inflow and hence ingestion as a possibility, this would require a large pressure gradient across the seal however which would tend to oppose ingestion.

The variation of loss generation with rotational speed was also assessed. A quantitative measure of loss generation in terms of entropy generated in the wheelspace is used. The entropy generated due to irreversibilities can be directly linked to a loss in the ability to do useful work. Since the overarching goal of this research is improvement of the efficiency of the machine, this measure of lost work is particularly

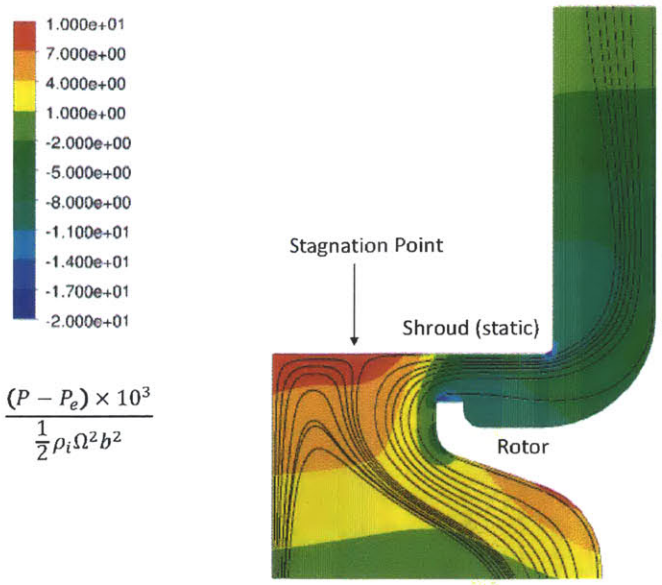

Figure 3-6: *Streamlines and pressure field contours for* $Re_\Phi = 2.5\times10^6$. *A radial stagnation point is formed on the outer surface of the shroud due to the circulatory flow structure in the wheelspace.*

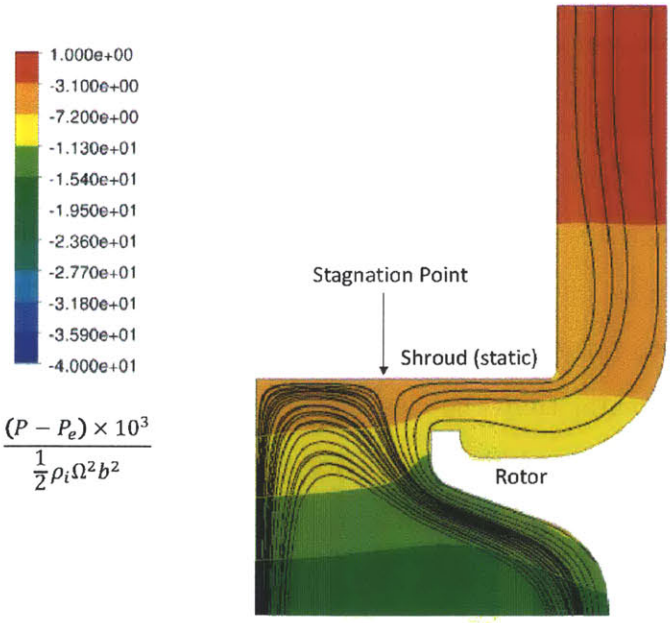

Figure 3-7: *Streamlines and pressure field contours for* $Re_\Phi = 1.1 \times 10^7$. *The stagnation point is now further aft (towards seal) than with* $Re_\Phi = 2.5 \times 10^6$.

useful.

To determine entropy generation, a control volume is drawn around the system. If we measure the entropy flux into and out of the system, the generation rate must be the difference between these two:

$$\dot{m}_{out}s_{out} - \dot{m}_{in}s_{in} = \dot{S}_{gen} \tag{3.1}$$

Evaluating this for the rotational speeds examined, the non-dimensionalized entropy generation rate is plotted against rotational Reynolds number in Fig. 3-8. This chart shows a steady increase in entropy generation with rotational speed.

To examine the sources of loss, a plot of local viscous entropy generation rate is shown in Fig. 3-9. This contour plot shows clearly the large entropy generation (read loss) generated in the rotor boundary layer, there is also noticeable generation in the separation zones off sharp edges in the seal region. This finding that the bulk of the entropy generation is contained in the rotor boundary layer is consistent with the findings of Fig. 3-8. The shear stress in the boundary layer increases with rotational speed (as the velocity difference between rotor surface and core increases) and thus the entropy generation due to viscous dissipation would also be expected to increase with rotational speed. This is exactly what is shown in Fig. 3-8.

Response to Varied Mass Flow

The net purge flow rate is the key parameter of interest and as such the impact of varying massflow rates is of interest. To assess this impact the steady, uniform axisymmetric model was run with varying supplied mass flow rates.

The results of this study were similar to those of the rotational speed. As the mass flow was decreased the stagnation point described above tended to move closer to the seal. Still, as in the rotational speed study, no ingestion was observed for any value of supplied mass flow rate, this further implies that rotation alone cannot drive ingestion in a radial seal configuration, some additional driver such as circumferential variation of the flowpath boundary condition must also be present.

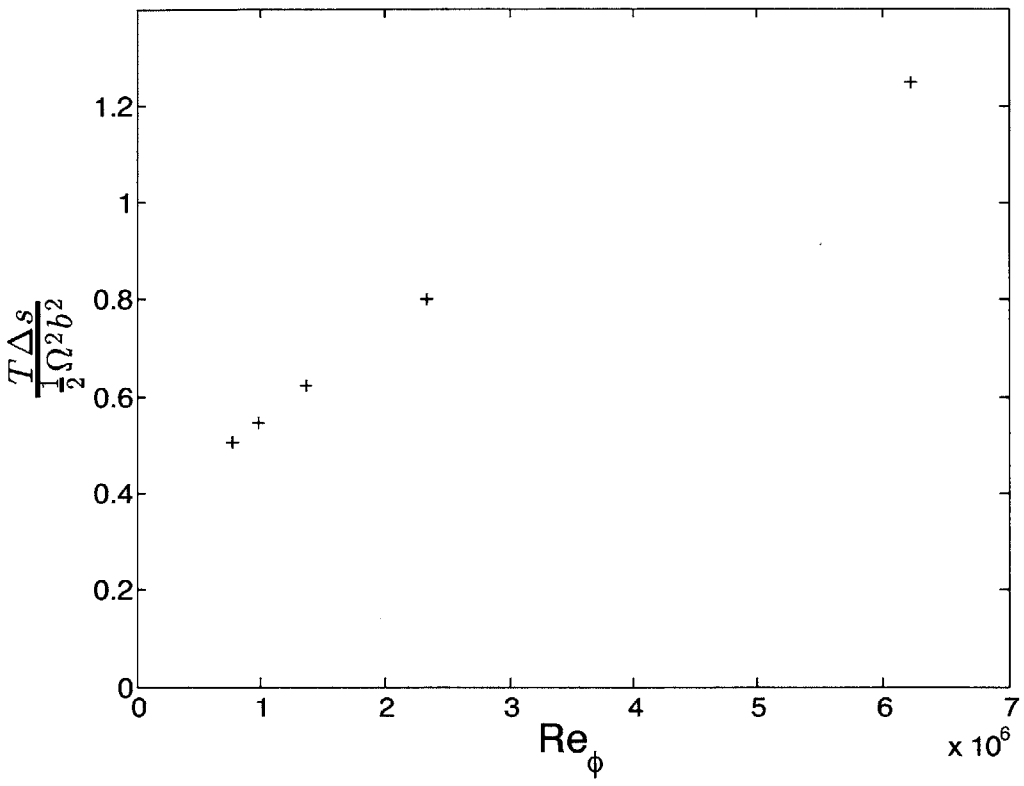

Figure 3-8: *Specific Entropy Flux vs. Rotational Speed. Steady increase in entropy generation in the wheelspace with rotational speed.*

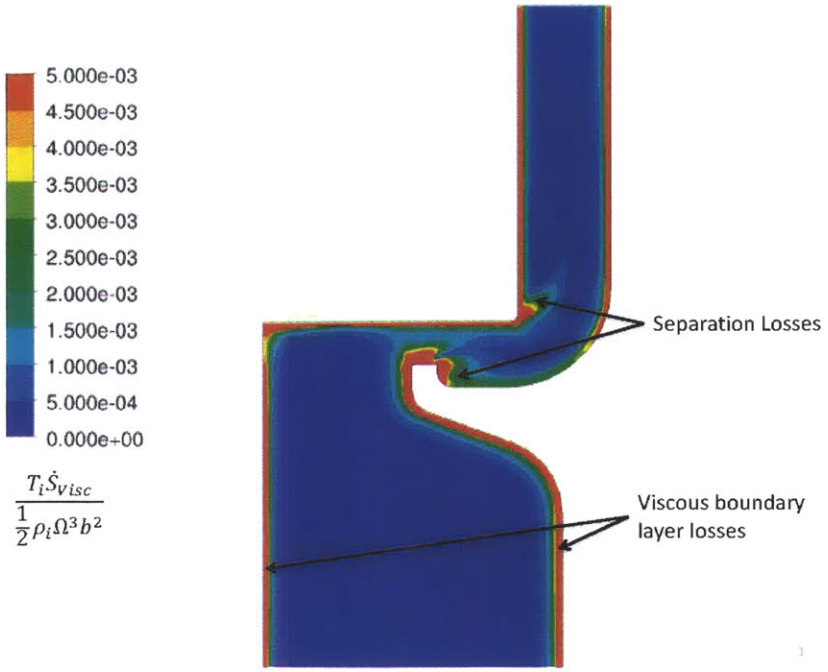

Figure 3-9: *Contours of viscous entropy generation for* $Re_\Phi = 2.5 \times 10^6$. *The primary regions of entropy generation are in the rotor/stator boundary layers and in the seperation zones.*

Response to Reduced Axial Overlap of Seal

Another parameter of interest is the axial overlap of the shroud over the seal tooth. To assess the impact of variation in overlap, the flow situation with the minimum overlap, (i.e. the edge of the seal tooth and the edge of the shroud are line-on-line) is analyzed. This geometry is shown in Fig. 3-10.

The results were similar to the baseline case examined (with overlap). As before, a radial stagnation point is formed on the shroud wall preventing ingestion, as the speed increases this stagnation point moves aft along the stator. In no cases among the cases analyzed did the stagnation point move outside of the seal. Streamlines for several rotational speeds are shown in Fig. 3-11, elucidating the movement of the stagnation point as rotational speed is increased.

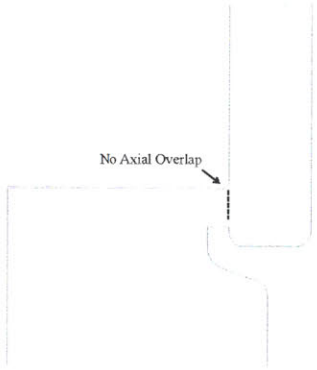

Figure 3-10: *Modified seal geometry: no axial overlap*

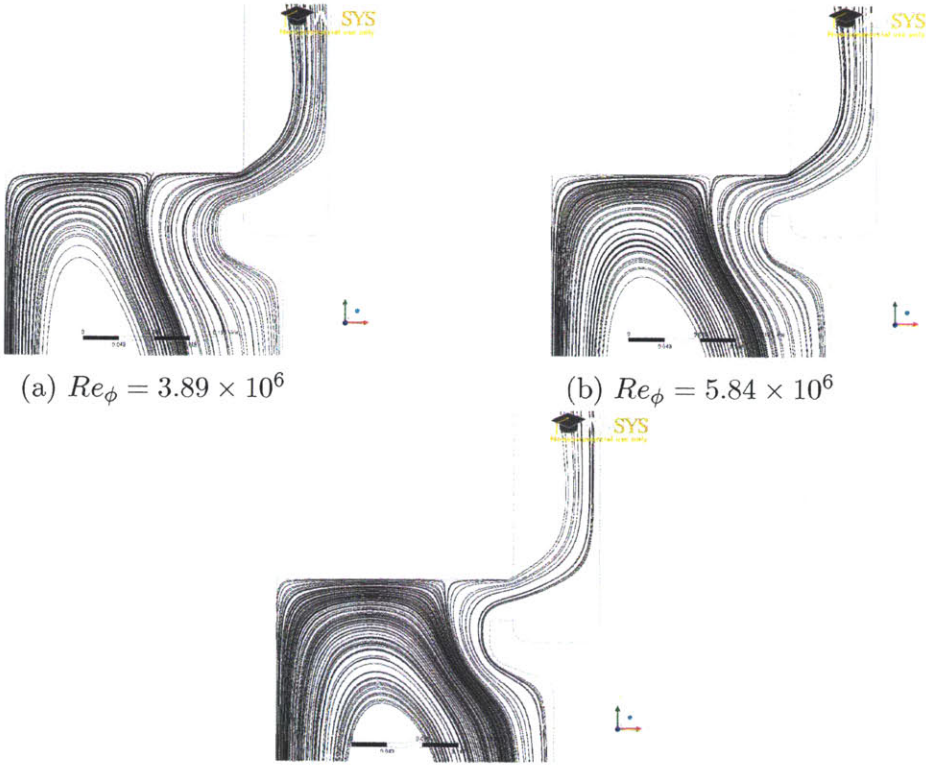

(a) $Re_\phi = 3.89 \times 10^6$

(b) $Re_\phi = 5.84 \times 10^6$

(c) $Re_\phi = 1.18 \times 10^7$

Figure 3-11: Streamlines with increasing rotational speed, no axial overlap.

Wheelspace Cavity Flow Response to Externally Imposed Pressure

A quantitative assessment of the response of wheelspace flow to the exit static pressure level was also performed. In the assessment the outlet pressure is first taken to be uniform and axisymmetric. The steady state model was analyzed for a series of static pressure levels to assess the impact of varying the "DC" pressure level. This study showed that the pressure field inside of the cavity is simply scaled by the outlet pressure ratio. This is true as long as the supply seal remains choked. While the seal is choked, the mass-flow through the system is fixed, regardless of backpressure. The pressure gradients in the cavity itself result from the radial throughflow (which is fixed) and the rotation rate in the cavity, which is independent of the pressure level. For a choked supply seal, the flowfield is therefore independent of the backpressure level. The implication of this is that ingestion cannot be driven by a quasi-steady raising of the backpressure.

Summary of Key Findings for Imposed Axisymmetric Pressure Field

Several specific results of engineering interest can be inferred for flow situations with steady axisymmetric backpressure. First, in a radial seal configuration, a radial stagnation point is set up where the flow that is pumped up the rotor impinges on the outer shroud. This creates a local high pressure zone at the seal that is ingestion resistant.

Second, with the inlet flow choked, varying external pressure level (on a quasi-steady basis) will not lead to ingestion. The absolute value of the pressure field in the cavity scales up or down with the external pressure but the flow structure remains the same.

3.2.2 Unsteady Axisymmetric

We now proceed to assess the response of wheelspace cavity flow when it is subjected to a uniform, axisymmetric back-pressure that is varying with time. The input frequency applied is sinusoidal. The frequency was varied over a range from 0 to several

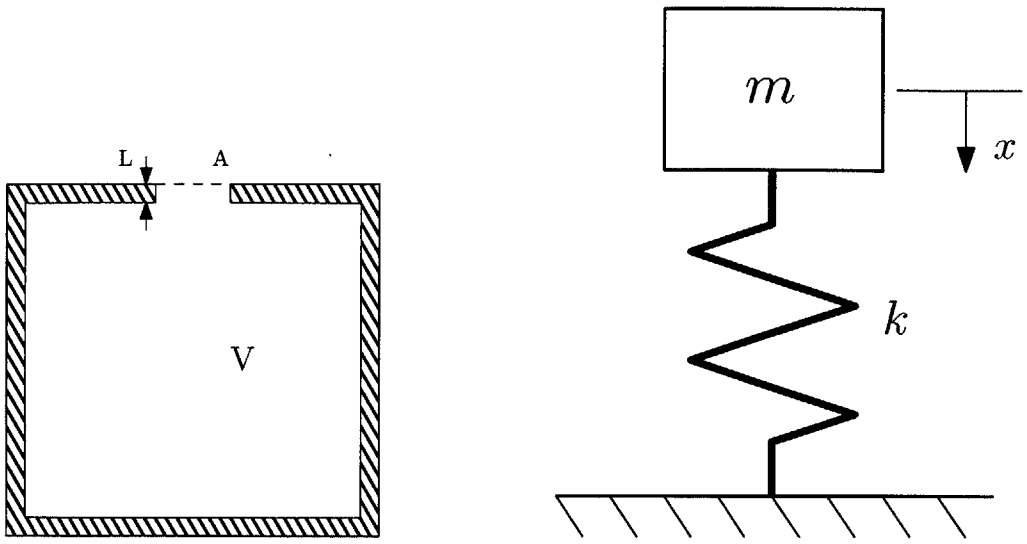

(a) A Helmholtz resonator (b) Analogous spring-mass model

Figure 3-12: Helmholtz resonator spring-mass analogy.

times the blade passing frequency.

The wheelspace and rim seal system has a number of characteristics in common with a canonical Helmholtz resonator (Fig. 3-12). A Helmholtz resonator consists of a large open plenum (the wheelspace) with a narrow "neck" (the rim seal). A key assumption of the Helmholtz resonator is that the pressure is uniform throughout the plenum at all times. This requires that the plenum be acoustically "compact", i.e. that the wavelength of the harmonic oscillation be much longer than the characteristic length of the plenum.

An analogy can be drawn between a Helmholtz resonator and a mass spring oscillator. The capacitance of the plenum provides the stiffness, k, and the air in the neck the mass. A schematic of this analogy can be seen in Fig. 3-12. Writing out the equations of motion yields the familiar mass-spring system equation for simple harmonic motion, equation 3.2.

$$m\ddot{x} = -kx \tag{3.2}$$

Assuming isentropic disturbances, and using the assumption that the pressure inside the plenum is uniform at all times, the capacitance of the plenum (k in equation 3.2)

Table 3.1: Calculated Helmholtz frequencies of the Trench and Wheelspace Cavities

Cavity	$\frac{\omega b}{a}$
Trench	72
Wheelspace	10.7

is given by equation 3.3.

$$k = \frac{\rho \bar{a}^2 A^2}{V} \tag{3.3}$$

The mass in the neck is simply $m = \rho AL$. Combining these in equation 3.2 yields a second order ordinary differential equation, equation 3.4 describing the Helmholtz resonator.

$$\ddot{x} = -\bar{a}^2 \frac{A}{LV} x \tag{3.4}$$

Solving for the eigenvalues of this equation gives the natural frequency of oscillation as.

$$\omega_n = \bar{a}\sqrt{\frac{A}{LV}} \tag{3.5}$$

Equation 3.5 provides a simple means of predicting the natural frequency of a Helmholtz resonator. It is important to note that in actuality the inertia of the "mass" element is greater than simply the mass in the neck. This is because in its oscillation the air must also move the air just inside and outside the neck. This is often corrected using an "effective" length of the neck rather than the physical length. In this analysis the physical neck length is used as the purpose is not obtaining an exact number, but rather identification.

The trench cavity can also be viewed as a Helmholtz resonator. The rim seal again forms the neck, and the outlet of the trench can be considered as being effectively closed by the main-path streamlines. This forms a Helmholtz resonator. The non-dimensional Helmholtz frequencies for the two cavities is shown in Table 3.1.

The results of this study are shown in figures 3-13 and 3-14, which show the pressure response just downstream of the seal, and the massflow response through the

seal respectively. The results in figure 3-13, a plot of pressure amplitude normalized by the pressure amplitude at the exit vs. frequency normalized by the calculated Helmholtz resonance frequency of the trench cavity, show that there are several large resonances. One such resonance occurs at the calculated value of trench Helmholtz frequency $\frac{\omega}{\omega_{trench}} = 1$ and another, smaller amplitude resonance, occurs near the calculated Helmholtz frequency of the wheelspace.

It is clear that the pressure field responds to the cavity natural modes, the natural follow up question is how the flow through the seal responds to this fluctuation in pressure field. Figure 3-14 shows the amplitude of oscillation in massflow rate (essentially velocity response) through the seal plotted vs. the reduced frequency of the seal which is defined as $\frac{\omega L}{U}$ where $U = \frac{\dot{m}_p}{\rho A_{seal}}$. As can be seen from figure 3-14, there is a strong flow response to the high frequency resonance, and with the reduced frequency lowered from unity to vanishing values the flow response again increases. This behavior can be explained by examining the role of reduced frequency in unsteady flow in a channel. In essence, the seal can be viewed as an annular duct, for the purposes of this analysis we assume that the upstream (wheelspace) total pressure is fixed. A detailed derivation of equation 3.6 is given in Appendix B.

$$\frac{u'}{\frac{p'}{\rho \bar{u}}} = \frac{i\beta - 1}{1 + \beta^2} \tag{3.6}$$

This is plotted in Figure 3-15. It is clear from this figure that as the reduced frequency is increased, the magnitude of the velocity response to the pressure fluctuation decreases to zero. In other words at some point the pressure field is oscillating so quickly that the inertia of the fluid cannot respond. At low values of reduced frequency however, the mass flow responds directly (quasi-steadily) to the pressure perturbation. Looking back at figure 3-14, we can see that the high frequency massflow response is minimal except at or near the resonance condition. At reduced frequencies below unity however it begins to increase again, this corresponds to the region where it begins to respond quasi steadily.

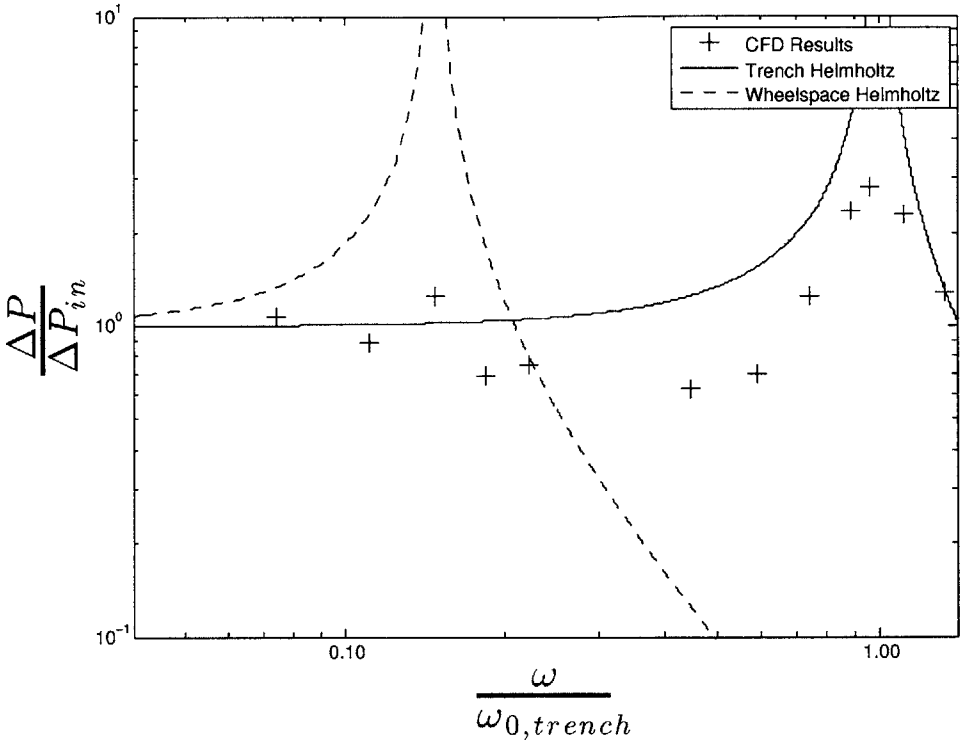

Figure 3-13: *Pressure Response to Axisymmetric External Oscillation. The crosses represent the calculated values. The dashed line represents the frequency response of an undamped Helmholtz oscillator corresponding to the wheelspace cavity. Similarly the solid line represents an undamped Helmholtz oscillator at the trench frequency. The CFD results show strong pressure response at both calculated Helmholtz Frequencies.*

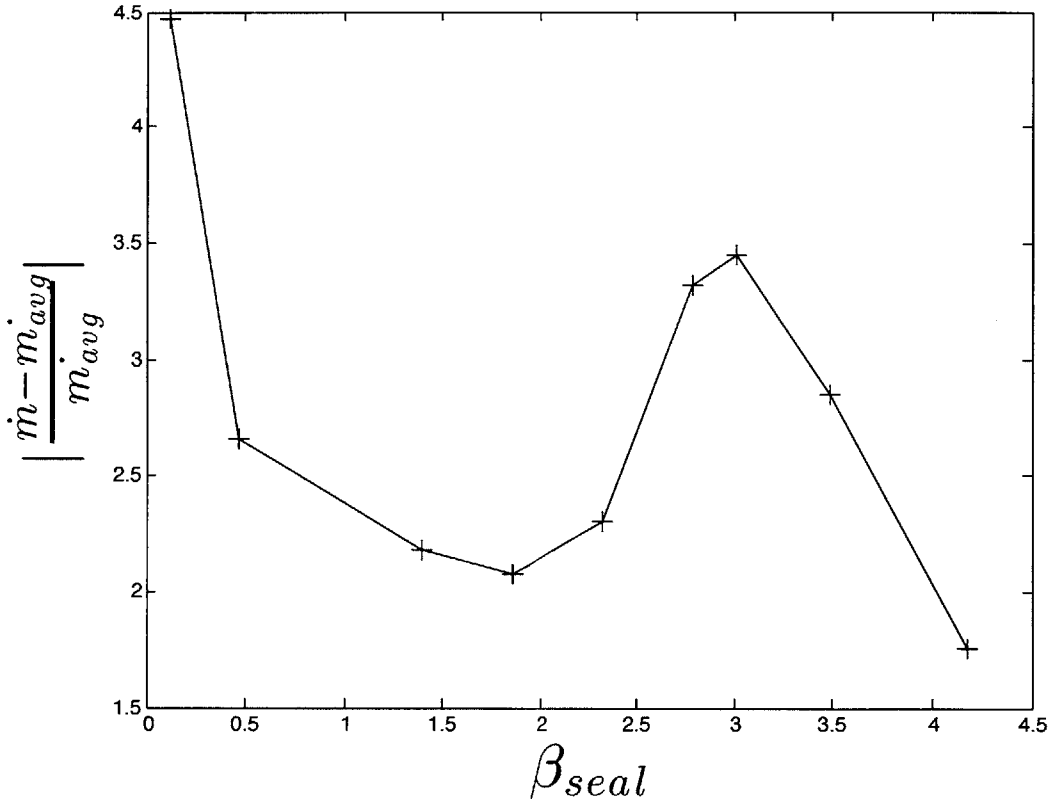

Figure 3-14: *Mass-Flow Response to Axisymmetric External Oscillation*

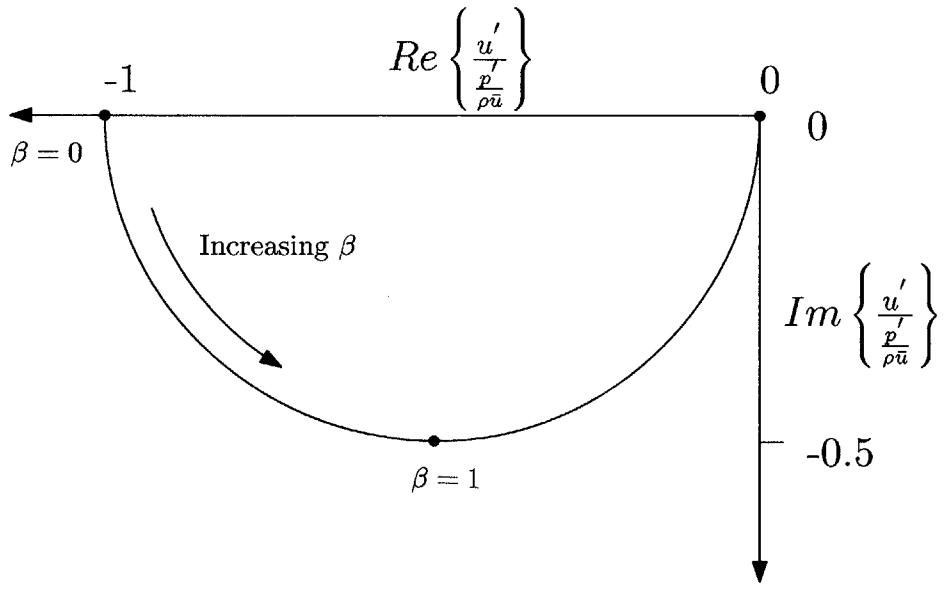

Figure 3-15: *Velocity perturbation due to fluctuation in the exit pressure for a straight duct as a function of reduced frequency.*

Summary

The results of this study demonstrate that unsteadiness can significantly impact sealing. At cavity resonance frequencies (such as Helmholtz) amplification of pressure field oscillations can lead to large amplitude oscillations of massflow through the seal (i.e. ingestion). This calls for the need to quantify the role of all the potential cavity modes on hot gas ingestion into the wheelspace.

3.2.3 Steady Circumferentially Periodic Pressure Field

We next assess the response of the wheelspace cavity flow to a steady, circumferentially periodic outlet pressure. This pressure field is representative of the influence of a row of stationary nozzle guide vanes (NGVs). The key parameter of interest in this study is the NGV spacing which defines the wavelength (λ) of the disturbance and the amplitude of the pressure variation in the circumferential direction.

Through the study it was found that this pressure disturbance can cause ingestion across the seal if it is strong enough at the location of the seal. In order to drive ingestion across the seal the maximum pressure disturbance amplitude just downstream of the seal must exceed the dynamic pressure in the seal (i.e. downstream static pressure higher than upstream total pressure). Understanding what sets the strength of the pressure disturbance downstream of the seal is therefore critical.

The key parameter in determining this disturbance was found to be the ratio of the trench depth to the disturbance wavelength. This decay is shown in figure 3-16, and is in accord with the theoretical decay rate based on the solution of the Laplace equation. The pressure disturbance downstream of the seal can therefore be primarily viewed as a function of the parameter $\frac{L}{\lambda}$ where L is the trench depth.

The impact of this on sealing effectiveness can be seen in Fig. 3-17a and Fig. 3-17b which show contour plots of "hot gas" concentration. This is computed by creating a tracer property which is convected with the flow and has a value of 1 ("hot gas" only) at the outlet and 0 ("cold gas" only) at the inlet. Intermediate values therefore represent mixes of hot and cold gas. It is clear from these figures that in the

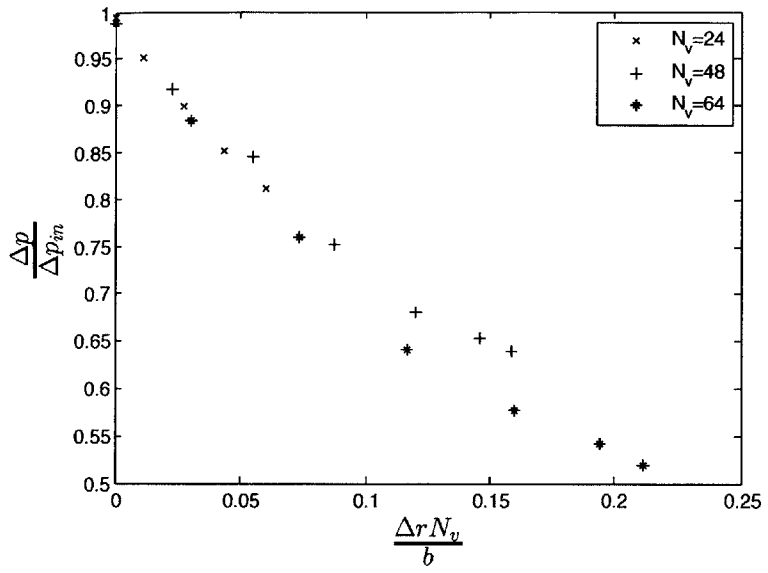

Figure 3-16: *Decay of pressure disturbance as a function of the ratio of depth to NGV pitch for three different NGV spacings. By casting in terms of the ratio of depth to NGV pitch, the three curves collapse and exhibit exponential decay.*

"deep trench case" corresponding to a value of $\frac{L}{\lambda} = 0.26$ there is no hot gas ingested across the seal whereas with $\frac{L}{\lambda} = 0.16$ there is. Both cases have the same amplitude of pressure disturbance at the outlet.

A more comprehensive study combining variation in the amplitude of the outlet pressure variation as well as the disturbance wavelength was also performed. Three wavelengths (corresponding to 24, 48, and 64 vanes) were examined at 4 values of disturbance pressure amplitude. The results of this study are shown in Fig. 3-18 which shows the ratio of the ingested massflow to net purge flow plotted against an estimate of the pressure amplitude at the seal. Based on the results discussed above, the amplitude of the disturbance is assumed to decay as the solution to Laplace's equation, i.e.

$$\Delta C_{p_{seal}} = \Delta C_{p_{in}} e^{-\frac{L}{2\pi\lambda}} \tag{3.7}$$

And, recognizing that for a periodic disturbance linked to the NGVs, $\lambda = \frac{2\pi R}{N_v}$, The disturbance amplitude at the seal can be written as:

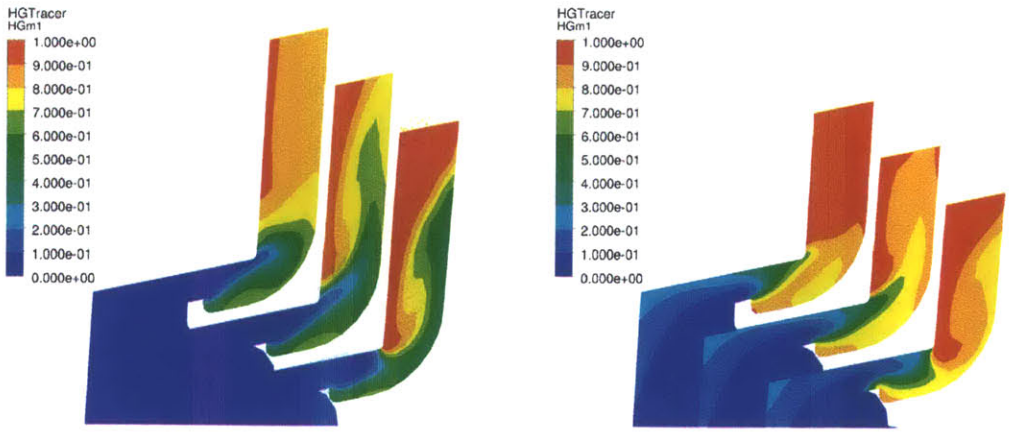

(a) "Deep" Trench, $\frac{L}{\lambda} = .26$ (b) "Shallow" Trench, $\frac{L}{\lambda} = .16$

Figure 3-17: Contours of "Hot Gas" ingestion for shallow and deep trenches.

$$\Delta C_{p_{seal}} = \Delta C_{p_{in}} e^{-\frac{L}{R} N_v} \tag{3.8}$$

Under the assumption that the ingestion ratio is a function of the magnitude of the pressure disturbance just downstream of the seal this is therefore used as the abcissa of figure 3-18. The figure demonstrates that using this method, the data from the three different wavelengths collapses to nearly the same curve. The functional dependence of the ingestion ratio can thus be cast in terms of the pressure variation amplitude immediately downstream of the seal and the ratio of trench depth to the vane pitch. The slight variation is likely due to the effect of swirl and curvature. We have assumed here that $\frac{L}{R} << 1$, i.e. a rectilinear (rather than annular) flow domain with no mean flow.

Summary of Key Findings

Circumferential variation in the external pressure field can lead to ingestion, whether this occurs is dependent on the amplitude of the disturbance pressure and the ratio of the trench depth to the wavelength of the disturbance which sets the magnitude of this pressure disturbance downstream of the seal. In other words, the ingestion ratio is functionally dependent on the disturbance wavelength and the imposed pressure disturbance amplitude.

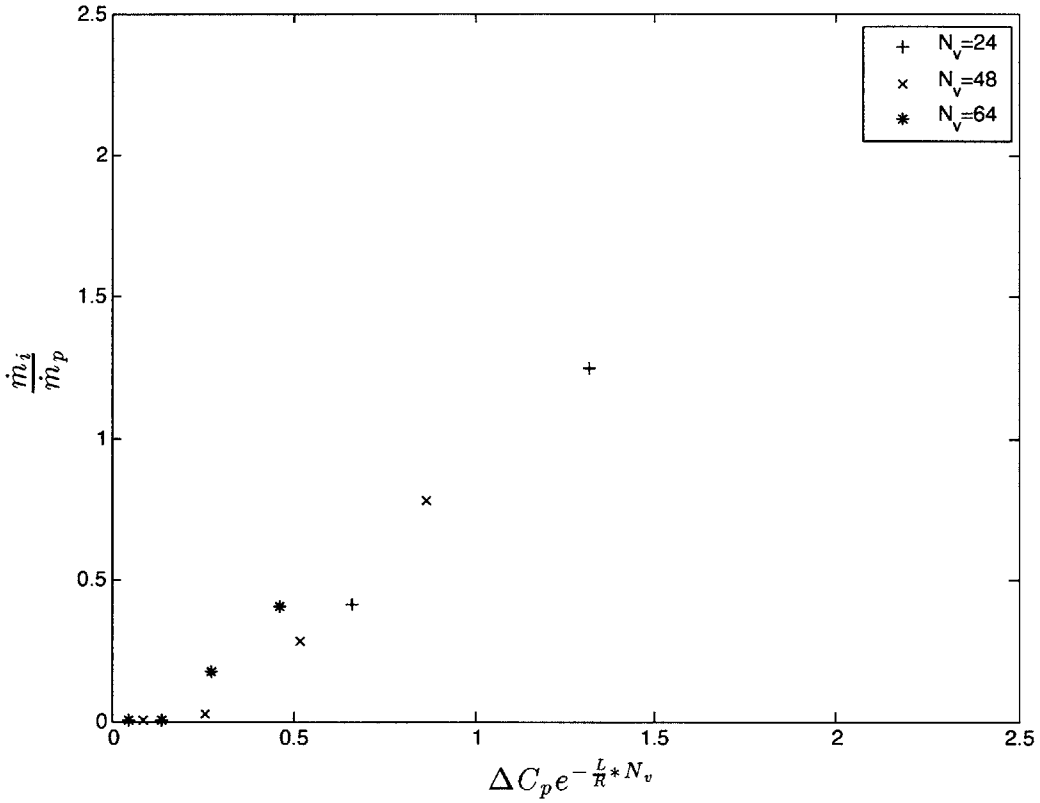

Figure 3-18: *Ratio of ingested mass flow to net purge flow as a function of pressure amplitude with 24, 48, and 64 vanes*

3.2.4 Unsteady Circumferentially Periodic Pressure Field

After analyzing the impact of a steady circumferentially periodic distribution (NGV) the next logical step is to assess the impact of an unsteady circumferentially periodic distribution, i.e. a circumferentially periodic traveling wave. This pressure distribution is representative of the pressure field associated with the bow waves generated by the rotating blade row.

The results of this study can be seen in figure 3-19 which shows the ratio of ingested to purge flow, normalized by the value of this ratio with a stationary periodic distribution, plotted against the ratio of wave speed to rotor speed $\frac{\omega}{\Omega}$. The interesting result of this is that as the rotor speed and wave speed travel in the same direction the ingested mass flow ratio increases, conversely when they counter-rotate the ingested flow decreases. The implication is that the closer the cavity swirl velocity is to the velocity of the pressure disturbance the worse the sealing effectiveness is. This same response was observed by Zlatinov [14] who explained the phenomenon through a linearized analysis and the mechanical analog of a simple harmonic oscillator.

One possible, physical, explanation for this phenomenon is that as $\frac{\omega}{\Omega}$ approaches unity, the disturbance frequency perceived by a particle traveling with the fluid tends to zero and the flow responds quasi-steadily. As $\frac{\omega}{\Omega}$ moves away from unity, the perceived reduced frequency increases, leading to a decrease in the velocity response, i.e. ingestion (this follows from argument similar to that of the preceding paragraph). A comparison of the velocity response across a sector of the seal is plotted in figure 3-20 as non-dimensional axial velocity through the seal vs. theta position, this clearly shows that as the swirl in the cavity and disturbance speed become closer, the velocity response is amplified (see Zlatinov [14] for more information on this phenomenon).

Summary of Key Findings

This set of calculations confirmed the previously obtained result that synchronization between swirl in the cavity (i.e. rotor speed) and the phase velocity of the imposed pressure field can lead to increased magnitude flow response. This suggests that

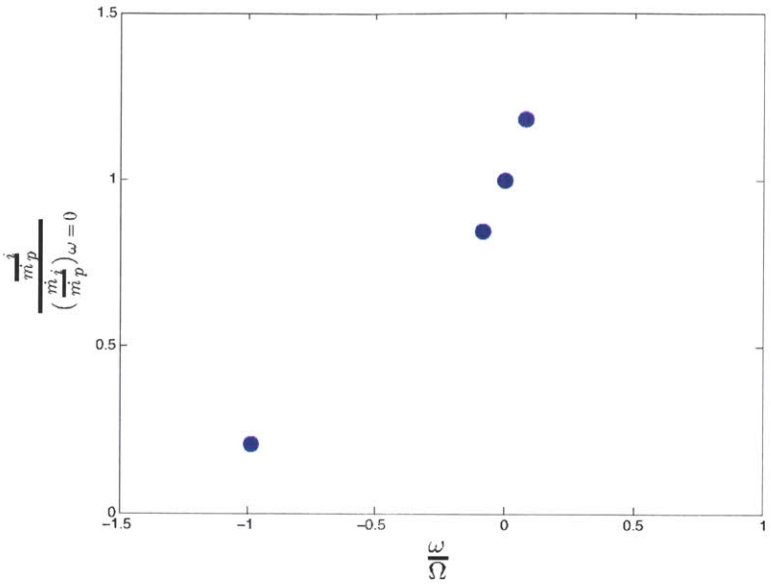

Figure 3-19: *Flow Response with varied swirl direction, periodic traveling wave. As the disturbance speed approaches the swirl velocity the seal ingestion response increases.*

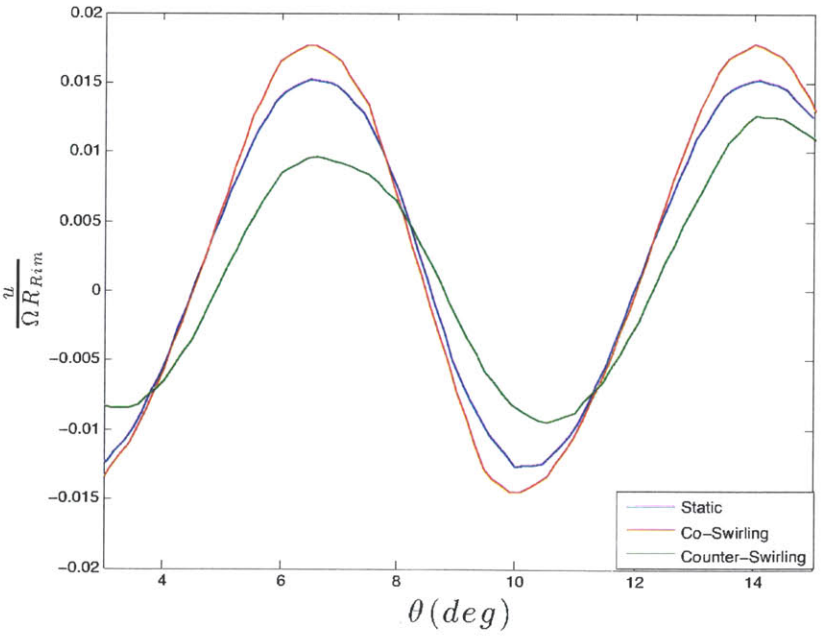

Figure 3-20: *Seal velocity response with varied swirl rate. The velocity response of the fluid in the seal is greater when the swirl velocity and the velocity of the disturbance are closer together (co-swirling).*

increasing the difference in velocity between the disturbance and the fluid could be a means of improving sealing effectiveness. The results of Zlatinov, however, showed that this increases the losses incurred when the purge flow is reintroduced into the flowpath. Thus there is a trade-off between minimizing loss generation and increasing sealing effectiveness that must be addressed at the system level.

3.3 Overall Summary

A number of studies were performed on a simple model of a canonical wheelspace/rim seal system. These studies assessed the parametric impact of varying rotational speed, mass flow, seal position, and turbine flowpath pressure boundary conditions. From these studies it was shown that varying rotational speed alone is not sufficient to induce ingestion in a steady flow. A radial stagnation point forms at the outer radius which acts to prevent ingestion.

Forcing the cavity with an unsteady flowpath pressure boundary condition demonstrated that there do exist resonance frequencies at which the pressure and massflow disturbances in the cavity can grow quite large resulting in unsteady ingestion into the wheelspace. Resonances were observed at frequencies corresponding to the cavity and trench Helmholtz frequencies.

Adding the additional complexity of periodic circumferential variation of the flowpath pressure boundary condition demonstrated that such variation can drive ingestion. The dependence of the ingestion flow rate on the static pressure field, such as that imposed by a cascade of nozzle guide vanes was shown to depend on the amplitude of the pressure variation just downstream of the seal itself. This amplitude is a function of the input pressure disturbance C_p and the ratio of the trench depth to the nozzle guide vane spacing (the disturbance decay length scale). If the circumferentially periodic pressure distribution was made to rotate (such as the situation of a rotating blade row). The computations confirmed the results previously observed by Zlatinov that a closer match between the phase speed of the disturbance and the swirl of the cavity flow leads to larger ingestion response.

Chapter 4

Small Disturbance Analysis

While the incremental computational approach described in chapter 2.1 provides a useful tool for analyzing and establishing parametric impacts, it requires lengthy unsteady analyses to be performed and is somewhat cumbersome. To simplify the task of assessing natural cavity modes a small disturbance flow analysis of the wheelspace rim cavity flow was formulated. This small disturbance formulation would provide a flexible framework for determining the cavity natural frequencies and modes followed by assessing their impact on ingestion. Thus it serves to complement the computational studies presented in Chapter 3.

The goal of this analysis is to develop a direct tool for assessing the natural frequencies and mode shapes of a canonical wheelspace geometry. Doing so will provide an ability to guide CFD analysis by identifying, a priori, the expected resonances so that the CFD can be accordingly designed to assess their impact on ingestion. Another anticipated benefit provided by the small disturbance analysis is that it directly gives the parametric dependencies and characterizing parameters. If appropriately non-dimensionalized, this formulation should provide the means to identify the key parameters controlling the cavity resonance frequencies.

In its most general form the small disturbance flow analysis could also be used as a means of analytically assessing the likelihood of ingestion. By solving the system subject to an arbitrary imposed pressure field, the point where $\frac{v'}{\bar{v}} = -1$ indicates the onset of ingestion, i.e. the disturbance velocity exactly counteracts the mean flow. In

this approach as in the natural mode assessment, the controlling parameters can be extracted directly from the formulation.

4.1 Generalized Formulation

We first seek a generalized formulation of the equations governing the flow within the wheelspace which can then be applied to specific cases to assess the natural modes of the system.

We start by writing out the governing equations, first, the momentum equation

$$\rho \frac{D\mathbf{v}}{Dt} = -\nabla p + \nabla \cdot \tau + \mathbf{X} \tag{4.1}$$

where τ represents the shear stress tensor and $\mathbf{X}$ represent body forces. The results of Batchelor demonstrate that under typical conditions in a gas turbine wheelspace cavity, the flow is characterized by an inviscid core rotating in solid body rotation. This allows us to drop the viscous stress terms. Likewise, working in the absolute frame, we can neglect body forces. This leaves us with the familiar euler equations:

$$\rho \frac{D\mathbf{v}}{Dt} = -\nabla p \tag{4.2}$$

Continuing, the conservation of mass can be expressed in differential form as:

$$\frac{D\rho}{Dt} + \nabla \cdot \rho\mathbf{v} = 0 \tag{4.3}$$

The equation of state ($p = \rho RT$) can be written in differential form as:

$$\frac{d\rho}{\rho} = \frac{dp}{p} + \frac{dT}{T} \tag{4.4}$$

using equation 4.4 we have:

$$ds = cp\left(\frac{dT}{T} + \frac{\gamma - 1}{\gamma}\frac{dp}{p}\right) \tag{4.5}$$

Assuming that the flow is isentropic we can write:

$$\frac{Ds}{Dt} = 0 \tag{4.6}$$

These equations can then be linearized by assuming a small disturbance (represented as prime quantities) on top of a base flow (represented as bar quantities).

$$() = \bar{()} + ()' \tag{4.7}$$

Equations 4.2 through 4.6 represent 6 equations in 6 unknowns and, given a specified base flow with appropriate boundary conditions can be solved to yield the disturbance flow.

In this general form, assuming only that the base flow is isentropic and axisymmetric, and that the disturbance entropy is uniform at the inlet, these equations can be combined to yield a single equation for the pressure disturbance.

$$\mathcal{A}(\mathcal{D}(p')) - \mathcal{B}(\mathcal{C}(p')) = 0 \tag{4.8}$$

Where we have defined the following linear operators to simplify representation:

$$\mathcal{L} = \frac{\partial}{\partial t} + \frac{\bar{v}}{r}\frac{\partial}{\partial \theta} + \bar{u}\frac{\partial}{\partial r} \tag{4.9}$$

$$\mathcal{A} = \frac{1}{\bar{a}^2}\mathcal{L} + \bar{u}\frac{d(\bar{a}^{-2})}{dr} + \frac{1}{2\bar{v}}\frac{\partial^2}{\partial\theta\partial r} \tag{4.10}$$

$$\mathcal{B} = \bar{\rho}\frac{\partial}{\partial r} + \frac{1}{r}\frac{d(\bar{\rho}r)}{dr} + \frac{\bar{\rho}}{2\bar{v}}\frac{\partial}{\partial\theta}\mathcal{L} \tag{4.11}$$

$$\mathcal{C} = \left(\mathcal{L} + \frac{\bar{u}}{r}\right)\left(\frac{r}{2\bar{v}}\left(\frac{1}{\bar{\rho}}\frac{\partial}{\partial r} - \frac{1}{\bar{\rho}^2\bar{a}^2}\frac{d\bar{p}}{dr}\right)\right) + \frac{1}{\bar{\rho}r}\frac{\partial}{\partial\theta} \tag{4.12}$$

$$\mathcal{D} = \left(\mathcal{L} + \frac{\bar{u}}{r}\right)\frac{r}{2\bar{v}}\mathcal{L} + \frac{1}{r}\frac{d(\bar{v}r)}{dr} \tag{4.13}$$

To reveal the characterizing parameters we introduce the following non-dimensionalization of this governing equation. Non-dimensional quantities are represented by $()^\star$.

$$t^\star = t\Omega \tag{4.14}$$

$$r^\star = \frac{r}{b} \tag{4.15}$$

$$v^\star = \frac{\bar{v}}{V} \tag{4.16}$$

$$u^\star = \frac{\bar{u}}{U} \tag{4.17}$$

$$p^\star = \frac{p}{\rho\Omega^2 b^2} \tag{4.18}$$

Applying these to the above operators leads to the following nondimensional quantities:

1. The ratio of characteristic radial throughflow velocity to the characteristic tangential velocity: $\frac{U}{V}$.
2. The ratio of tangential velocity to rim speed: $\frac{V}{\Omega b}$
3. The ratio of radial throughflow velocity to rim speed: $\frac{U}{\Omega b}$
4. The rim Mach number: $\frac{\Omega b}{\bar{a}}$
5. The product of tangential Mach number and radial throughflow Mach number: $\frac{UV}{\bar{a}^2}$

For the purposes of identifying the natural modes of the wheelspace system these equations will be most useful when put in the form of an eigenvalue problem. To do this, we first cast the disturbances in normal mode form, recognizing that disturbances are circumferentially periodic. The hat quantities are functions of radius only.

$$()' = \hat{()}e^{-j\omega t + k\theta} \tag{4.19}$$

Substituting this into the above equations we obtain a systems of equations for k and ω as well as the hat quantities that is independent of θ and time; this set of equations constitutes a dispersion relation relating k and ω (or equivalently an eigenvalue problem for ω).

4.2 Results

In the following sections we apply the analysis formulated above to several simple base flows constituting the simplest representations of the flow in the wheelspace. Through these assessments the role of the characterizing parameters can be elucidated. The results of these calculations are then assessed against experimental observations.

4.2.1 Solid Body Rotation without Throughflow

We can apply the generalized formulation above by assuming a mean flow. The case described here is representative of a cavity with Batchelor type flow, where all of the outflow occurs in the boundary layers and the bulk of the cavity is characterized by an inviscid core in solid body rotation. To simplify the analysis we assume that the base flow is incompressible. It is also assumed that disturbances and derivatives in the axial (x) direction are negligible, i.e. the flow is planar in the $R-\theta$ plane.

Using the non-dimensionalization of the preceding section, with $V = \Omega b$ and substituting the assumed base flow into eqn 4.8 in normal mode form, and defining the following characterizing parameters,

$$\beta_\Omega = \frac{\Omega b}{\bar{a}} \tag{4.20}$$

$$\beta_\omega = \frac{\omega b}{\bar{a}} \tag{4.21}$$

yields the following relation.

$$\left((k\beta_\Omega - \beta_\omega)^2 + 2\beta_\Omega^2\left(\frac{1}{1-\frac{\beta\omega}{k\beta_\Omega}} - 3\right) - \frac{k^2}{r^2}\right)\hat{p} + \left(\frac{1}{r} - \beta_\Omega^2\right)\frac{d\hat{p}}{dr} + \frac{d^2\hat{p}}{dr^2} = 0 \quad (4.22)$$

From this the characterizing non-dimensional parameters begin to emerge. It is clear that the primary driver of the non-dimensional frequency(β_ω) is the non-dimensional speed of rotation (tangential mach number at the rim). Another parameter that emerges from this is the ratio of the disturbance phase speed to the angular speed of the rotor disk $\frac{\omega}{k\Omega}$. We can further assess the role of these parameters by applying boundary conditions and solving the resulting eigenvalue equation.

First, if we assume that the wheelspace can be approximated as a narrow annulus, i.e. $(R_o - R_i << R_o)$, as shown in Fig. 4-2, we can approximate r in equation 4.22 by a mean radius R_m.

$$\left((k\beta_\Omega - \beta_\omega)^2 + 2\beta_\Omega^2\left(\frac{1}{1-\frac{\beta\omega}{k\beta_\Omega}} - 3\right) - \frac{k^2}{R_m^2}\right)\hat{p} + \left(\frac{1}{R_m} - \beta_\Omega^2\right)\frac{d\hat{p}}{dr} + \frac{d^2\hat{p}}{dr^2} = 0 \quad (4.23)$$

This is now a second order ordinary differential equation with constant coefficients which has the solution

$$\hat{p} = e^{\lambda_1 r} + e^{\lambda_2 r} \quad (4.24)$$

where λ_1 and λ_2 are found by solving the characteristic equation:

$$a\lambda^2 + b\lambda + c = 0 \quad (4.25)$$

If we make the assumption of a wall at the inner radius, and an opening at the outer radius we obtain the following boundary conditions:

$$\hat{p}(R_o) = 0 \quad (4.26)$$

$$\hat{u}(R_i) = 0 \quad (4.27)$$

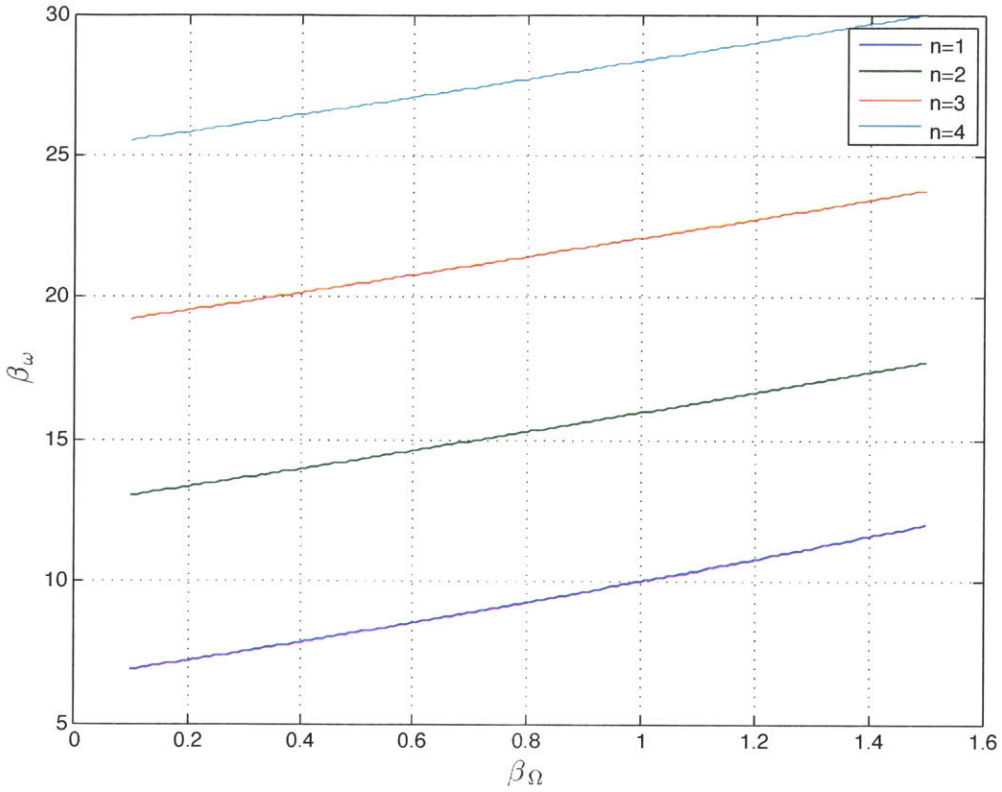

Figure 4-1: *Variation of β_ω vs. β_Ω for k=3 circumferential mode*

Using these boundary conditions along with equations 4.17-4.19 we obtain equation 4.22 and can solve for the natural frequencies β_ω of the system. The solution to this equation for the case where $k = 3$,$R_o = 1$,and $R_i = .5$ for a variety of radial mode numbers (n) over a range of β_Ω can be seen in Fig. 4-1. From this chart it becomes clear that increasing the rotational speed of the cavity tends to increase the natural frequency of the cavity, and it does so nearly linearly. As expected increasing n increases the frequency, these lines of constant radial wavenumber are nearly parallel to each other, showing the same dependence on the rotational speed.

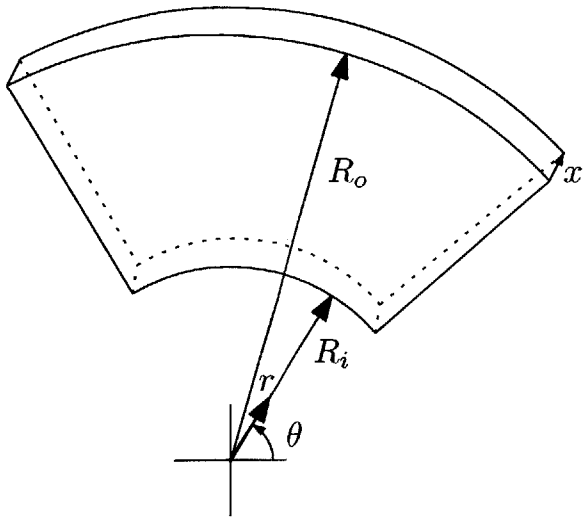

Figure 4-2: *Sketch of Annulus*

4.2.2 Without Rotation($\beta = 0$)

Perhaps the simplest case to analyze is what happens in the case where the swirl in the cavity is zero, i.e. no rotation. In this case equation 4.22 simplifies to:

$$((\bar{\omega}M)^2 - \frac{k^2}{r^2})\hat{p} + \frac{1}{r}\frac{d\hat{p}}{dr} + \frac{d^2\hat{p}}{dr^2} = 0 \tag{4.28}$$

This is a Sturm-Liouville equation, which has the well known solution:

$$\hat{p} = c_1 J_n(\bar{\omega}M) + c_2 Y_n(\bar{\omega}M) \tag{4.29}$$

where n is the radial wave number. J_n is an n^{th} order Bessel function of the first kind, and Y_n is an n^{th} order Bessel function of the second kind.

If we assume that the outer radius is open and the inner radius a rigid wall we impose the boundary conditions $p(\hat{R}_o) = 0$, i.e. no pressure disturbance at the outer diameter, and $\frac{d\hat{p}}{dr} = 0$, i.e. no radial velocity at the inner diameter no flow through the wall). Applying these boundary conditions to equation 4.29 the resulting eigenvalue problem can be solved for the eigenvalues $\bar{\omega}M$.

Table 4.1: Comparison of Experimental and Predicted Frequencies for "Mercedes Star"

Method	$\frac{\omega b}{a}$
Measured [6]	1.0
Small Disturbance (no rotation)	3.7

4.2.3 Comparison to Experimental Data

Several experimental investigations have suggested the presence of low frequency modes. A computational study by Jakoby et al. modeled such a mode, showing a 3-lobe mode that rotated at just below wheelspeed. They dubbed this mode a "Mercedes Star" pattern and found a matching signal in the experimental measurements. The mechanism for the emergence of this pattern remained un-addressed however.

It stands to reason that such a three-lobe pattern is a natural mode of the system. To test this hypothesis Equation 4.28 was solved for the $k = 3$,$n = 1$ mode, which would correspond to such a pattern. This solution can be seen in Fig. 4-3. When compared against the results of Jakoby et. al, this 3^{rd} circumferential mode qualitatively bears many similarities, showing a similar 3 lobed system. A quantitative assessment is shown in Table 4.1 which compares the analytically determined natural frequency corresponding to this mode shape with the measured frequency reported. The calculated frequency is roughly three times what was measured. This indicates that while the calculated result is of the right order of magnitude, if this natural mode is the source of the experimental observation the simple case with no rotation and no throughflow does not fully capture it. If we extend the results of the preceding section (with rotation) to this test case, the system stiffens and the results move even further from the data suggesting rotation alone cannot bring closure with the data. Additional factors such as radial throughflow need to also be considered.

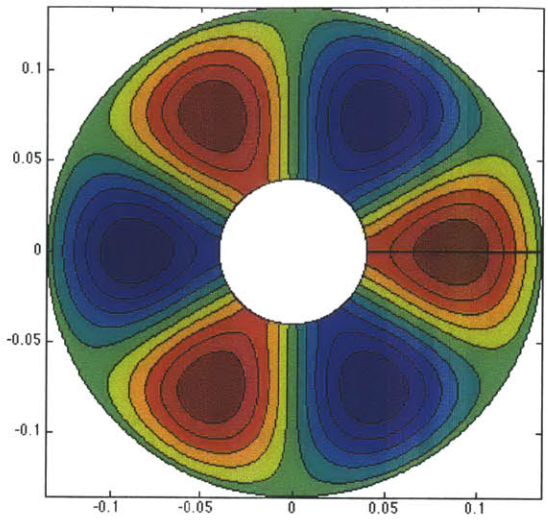

Figure 4-3: *Computed mode shape (pressure) for* $k = 3$, $n = 1$

4.2.4 Overall Summary

A small disturbance analysis of turbine wheelspace flow has been formulated for direct determination of eigen frequencies and associated eigen modes. The analysis also provides an alternative means to assess the unsteady non-axisymmetric flow disturbances in the wheelspace with a characteristic mean flow (radial swirling throughflow and temperature non-uniformity) in response to the pressure imposed by the turbine flow path. We inferred from the analysis the following non-dimensional characterizing parameters for the cavity modes:

1. The rim mach number: $\dfrac{\Omega b}{\bar{a}}$
2. The ratio of characteristic radial throughflow velocity to the characteristic tangential velocity: $\dfrac{U}{V}$.
3. The ratio of tangential velocity to rim speed: $\dfrac{V}{\Omega b}$
4. The ratio of radial throughflow velocity to rim speed: $\dfrac{U}{\Omega b}$
5. The product of the tangential and radial throughflow Mach numbers: $\dfrac{UV}{\bar{a}^2}$

6. The non-dimensional mean radius of the wheelspace: $\frac{R_m}{b}$

7. The compactness ratio based on the disturbance frequency: $\frac{\omega b}{\bar{a}}$

8. The ratio of the disturbance phase speed to the disk rotating speed: $\frac{\omega}{k\Omega}$

These parameters come directly from the non-dimensionalization of the above operators but are not all independent (note that items 3 and 4 can be combined to yield 2).

The analysis shows the existence of a three-harmonic circumferential rotating modes which is in accord with experimental measurements, though the calculated frequency with no mean flow is several times higher than measured. The addition of rotation moves the modes to higher frequencies corresponding to a stiffening of the system.

Chapter 5

Summary and Conclusions

5.1 Summary

The goal of this research is the characterization of the flow in the turbine rim cavity and wheelspace and the identification of the key drivers governing sealing effectiveness. Of particular interest is the role that resonance and natural cavity modes play which, to this author's knowledge, has not been addressed in the published literature to date.

To enable the completion of this goal a complementary computational and analytical framework was developed. The computational framework is based on the idea of implementing the level of physical complexity incrementally, and assessing the impact of each change on the flow field in the wheelspace and rim cavity. By doing so causal linkages can be formed that can later be assessed against experiment and used to expand the design space by quantitatively linking flow processes and their drivers to ingestion.

The other component of the framework is a modal analysis via a small disturbance formulation. The advantages to this approach are numerous. It allows for parametric studies to be performed much more directly than with an equivalent computational model. Perhaps its most powerful feature is its ability to bring the controlling parameters directly to the fore by the form of the equation.

Using these tools numerous analyses can be carried out to yield a quantitive understanding of the flow in the rotor stator wheelspaces of gas turbines.

5.2 Key Findings

The formulation of a computational model has allowed the assessment of the response of a characteristic wheelspace cavity to an imposed turbine flowpath pressure field. This has led to the following findings:

1. The assumption of constant (choked) supply flow has implications for the quasi-steady response of the wheelspace flow structure. With the inlet flow choked variations in the absolute level of the downstream pressure cause the wheelspace pressure field to scale up or down, but the flow structure and amount of purge flow remains the same. Because of this, quasi-steady variations in the axisymmetric pressure field do not lead to ingestion while the seal remains choked.

2. Circumferential variation in the external pressure field can lead to ingestion. This was assessed by imposing a periodic variation around the circumference of the rim. These studies identified the ratio of disturbance wavelength to trench depth as an important characterizing parameter.

3. Over a range of rotational Reynolds numbers of interest in gas turbines ingestion could not be driven for a steady axisymmetric turbine flow path pressure field by varying rotational speed alone. A key feature preventing ingestion is the formation of a stagnation point on the shroud. The flow that is pumped up the rotor boundary layer impinges on the outer shroud resulting in a local high pressure zone at the seal that resists ingestion.

4. Varying the purge flow rate, with an axisymmetric external pressure field, does not lead to the onset of ingestion. As was shown in the case of varying rotational speed, it appears there needs to be another driver, such as a non-axisymmetric external pressure field, to drive ingestion on a quasi-steady basis.

5. Unsteadiness and, in particular, resonance (the excitation of cavity modes) could have a significant impact on sealing effectiveness. An unsteady axisymmetric pressure field in the turbine main flow path induces strong responses

in both pressure and seal mass flow rate when frequencies corresponding to those of the natural cavity modes are imposed in the turbine main flowpath. It also suggests that the seal reduced frequency, defined as $\frac{\omega L_t}{U_{seal}}$ the ratio of the characteristic convection time through the seal to the unsteady timescale, is a characterizing parameter for ingestion. The influence of resonance on rim cavity sealing has not to this author's knowledge been addressed in the publicly available literature. Characterizing the natural modes of the system is an important step towards understanding an aspect of ingestion response.

6. An unsteady non-axisymmetric pressure field in the turbine main flow path, similar to the steady circumferential variation, can lead to ingestion. In this case however the ratio between the phase speed of the pressure field and the swirl in the wheelspace is an important parameter. This has been discussed in the literature and was confirmed in these studies.

A generalized small disturbance analysis of turbine wheelspace flow has been formulated for direct determination of eigen frequencies and associated eigen modes. We inferred from this analysis the following non-dimensional characterizing parameters for the cavity modes:

1. The rim mach number: $\frac{\Omega b}{\bar{a}}$
2. The ratio of characteristic radial throughflow velocity to the characteristic tangential velocity: $\frac{U}{V}$.
3. The ratio of tangential velocity to rim speed: $\frac{V}{\Omega b}$
4. The ratio of radial throughflow velocity to rim speed: $\frac{U}{\Omega b}$
5. The product of the tangential and radial throughflow Mach numbers: $\frac{UV}{\bar{a}^2}$
6. The non-dimensional mean radius of the wheelspace: $\frac{R_m}{b}$
7. The compactness ratio based on the disturbance frequency: $\frac{\omega b}{\bar{a}}$

8. The ratio of the disturbance phase speed to the disk rotating speed: $\frac{\omega}{k\Omega}$

These parameters come directly from the non-dimensionalization but it should be noted that they are not all independent (e.g. items 3 and 4 can be combined to yield 2).

For the situation of simple wheelspace flow consisting of no mean flow with non-rotating discs, the analysis shows the plausible existence of a three-harmonic circumferential rotating modes in accord with experimental measurements. The addition of rotation also shows the existence of these modes, but with higher frequencies corresponding to a stiffening of the system.

Chapter 6

Future Work

The research presented in this thesis addresses only a few selected aspects of the turbine wheelspace cavity flow. In this chapter we elaborate further the areas of planned future work.

First, the research described here has led to the development of a framework for assessing the response of the wheelspace cavity to various stimuli. As described in the preceding chapters a number of flow studies have been performed but there are many yet to be done to fully characterize the wheelspace flow and any attendant hot gas ingestion phenomena. Of particular interest would be the continued investigation of the low order natural modes seen in experiment and its assessment using the analytical small disturbance analysis, as well as through computational modeling. This will likely require introducing perturbation to excite these modes. If these can be recreated in the computations the impact on the flow field and sealing effectiveness can be readily determined.

Additionally, to give added credence to the results of the computational studies additional investigation of the impact of the many simplifying assumptions should be performed. One key assumption that has been identified for future study is the placement of the dump boundary pressure. Currently this is right at the interface between the main flowpath and the trench cavity. Previous work [8] has suggested that the shear layer that develops at this boundary and interaction of the main flowpath and the purge air could be important to ingestion. To address this the computational

domain can be extended to include in its control volume a piece of the flowpath such that it encompasses the interface region.

As described in the preceding chapters, one of the key findings of this effort to date has been that there can be cavity resonances that occur at frequencies of interest to gas turbine (of the order of the blade passing frequency) and that these resonances can result in significant flow response at the rim seal. An important aspect to investigate is whether these resonance modes are of practical importance to ingestion. In other words, it has yet to be established that the resonant responses identified are of a magnitude and structure such that they are a significant driver of detrimental ingestion. One question that should be answered to address this is what controls the penetration depth of air ingested due to resonance, i.e. is it all expelled from the cavity over the course of one period? Does it mix significantly to raise the cavity temperature? How does it get distributed throughout the cavity? This can be answered through computational modeling coupled with assessments against experiments. If the resonance modes can be recreated computationally, the time history of ingested flow can be examined to answer the above questions. These are all important questions to answer in order to address the question of what is the role of resonance in ingestion.

Along this line, another question to be addressed in future work is what sets the acceptable ingestion level. Current dogma suggests that no ingestion can be tolerated without compromising the design. It is not hard however to conclude that this may be an overly stringent criteria. The detrimental impact of ingestion is due to the raising of the metal temperatures of the components of interest. This temperature is a function of the heat load imposed by the flow in the wheelspace, i.e. a function of both the local air temperature of the air scrubbing the component and the heat transfer coefficients at that location. Therefore, in order to understand the impact of ingestion there are two key questions that must be answered: What is the distribution of ingested air in the wheelspace cavity? And what features drive heat transfer in the areas of interest? By answering these questions a quantitative determination of acceptable ingestion levels can be set based on a physically rigorous criteria. It is

possible that, armed with a quantitative understanding of the drivers of heat load, the designer could create a system that is tolerant to ingestion with negligible impact on durability.

The parametric studies performed here raise yet another question for continued study. It has been shown that ingestion is primarily a response to the pressure field imposed by the turbine flowpath design on the wheelspace system. This suggests the possibility that there exists a pressure field that is optimal for preventing ingestion and maximizing sealing effectiveness. A goal of future study would be to identify what this pressure field would be (under the constraint that it must still contain all the key components of the pressure field inherent to the turbine design). The identification of such a pressure field only represents a starting point for future research as it would raise detailed questions out of the scope of this effort of whether this could feasibly be made without compromising turbine efficiency.

Loss generation within the wheelspace and rim cavity is yet another aspect of characterizing the wheelspace rim cavity system that has yet to be addressed with any rigor. While much attention in previous literature has been paid to the losses associated with the interaction between the purge flow and main flowpath after it exits the rim cavity, little if any attention has been paid to the loss generation mechanisms inside the wheelspace and through the seal. One reason for this is that a conventional sealing process such as a clearance type seal inherently requires that there be losses associated with sudden expansion etc. Since, in the final analysis, the goal of this research is maximizing the efficiency of the gas turbine system it is important to identify and understand all of the individual sources of loss in the system and how they are related in order to minimize the total losses in the overall system. It would be beneficial to formulate a simple model incorporating all of the sources of loss associated with the purge flow. There have been results suggesting that there is a tradeoff between sealing effectiveness, and turbine efficiency. A simple model containing all of the sources of loss, could therefore be used to optimize the purge flow system as a whole for maximum cycle efficiency. Looking at each aspect individually is likely not the best approach.

Obviously one other critical piece of future work is assessing the results of all of this analysis against data and observation from rig and engine tests. As described in the section 1.1 there have been extensive wheelspace rig tests performed over the past thirty years, few however have focused on gathering the unsteady data required to to assess the role of cavity modes. Thus there is an opportunity to use the research results here to plan and ask what constitute good experiments to implement for advancing the science and engineering of modern turbine wheel space aero-thermal physics. For instance, the parametric controlling trends delineated in Chapter 4 of the various characterizing parameters on the cavity modes can be leveraged to yield results of utility for designing and implementing instructive computations and experiments.

Appendix A

Small Disturbance Analysis Derivation

We start the analysis from the Euler momentum equations, continuity, energy conservation, and equation of state outlined in chapter 4.

To linearize the equations we assume a steady base flow subject to unsteady perturbations of small amplitude.

$$() = \bar{()} + ()' \tag{A.1}$$

Substituting these in and neglecting products of disturbance quantities yields the following set of equations:

Continuity in radial coordinates:

$$\frac{\partial \rho'}{\partial t} + \frac{\bar{v}\partial \rho'}{r\partial \theta} + \bar{u}\frac{\partial \rho'}{\partial r} + \bar{\rho}\frac{\partial u'}{\partial r} + u'\frac{\partial \bar{\rho}}{\partial r} + \frac{u'\bar{\rho}}{r} + \frac{\bar{\rho}\partial v'}{r\partial \theta} + \bar{\rho}\frac{\partial w'}{\partial x} + w'\frac{\partial \bar{\rho}}{\partial x} = 0 \tag{A.2}$$

Conservation of Radial Momentum:

$$\frac{\partial u'}{\partial t} + \frac{\bar{v}\partial u'}{r\partial \theta} + \bar{u}\frac{\partial u'}{\partial r} + u'\frac{\partial \bar{u}}{\partial r} - \frac{2\bar{v}v'}{r} + w'\frac{\partial \bar{u}}{\partial x} = -\frac{1}{\bar{\rho}}\frac{\partial p'}{\partial r} + \frac{\rho'}{\bar{\rho}^2}\frac{\partial \bar{p}}{\partial r} \tag{A.3}$$

Conservation of Tangential Momentum:

$$\frac{\partial v}{\partial t}+\frac{\bar{v}\partial v'}{r\partial\theta}+\bar{u}\frac{\partial v'}{\partial r}+u'\frac{\partial\bar{v}}{\partial r}+\frac{u'\bar{v}}{r}+\frac{\bar{u}v'}{r}+w'\frac{\partial\bar{v}}{\partial x}=-\frac{1}{\bar{\rho}r}\frac{\partial p'}{\partial\theta} \tag{A.4}$$

Conservation of Axial Momentum

$$\frac{\partial w'}{\partial t}+\frac{\bar{v}\partial w'}{r\partial\theta}+\bar{u}\frac{\partial w'}{\partial r}=-\frac{1}{\bar{\rho}}\frac{\partial p'}{\partial x}+\frac{\rho'}{\bar{\rho}^2}\frac{\partial\bar{p}}{\partial x} \tag{A.5}$$

Entropy:

$$\frac{\partial s'}{\partial t}+\frac{\bar{v}\partial s'}{r\partial\theta}+\bar{u}\frac{\partial s'}{\partial r}+u'\frac{\partial\bar{s}}{\partial r}+w'\frac{\partial\bar{s}}{\partial x}=0 \tag{A.6}$$

$$s=c_p\left(\frac{T'}{\bar{T}}-\frac{\gamma-1}{\gamma}\frac{p'}{\bar{p}}\right) \tag{A.7}$$

Equation of State:

$$\frac{p'}{\bar{p}}=\frac{\rho'}{\bar{\rho}}+\frac{T'}{\bar{T}} \tag{A.8}$$

These can be further reduced by making the assumption that the disturbances are isentropic in nature. This allows us to put disturbance density in terms of disturbance pressure.

$$\rho'=\frac{1}{\bar{a}^2}p' \tag{A.9}$$

We also assume that axial velocities and disturbances are negligible since the radius is much larger than the rotor-stator spacing. This eliminates all of the $\bar{w}$ and w' and the derivatives in the x direction.

Applying these assumptions to the system of equations outline above yields 3 equations in 3 unknowns $(p', u', ')$.

$$\frac{1}{\bar{a}^2}\frac{\partial p'}{\partial t}+\frac{\bar{v}\partial p'}{r\bar{a}^2\partial\theta}+\frac{\bar{u}}{\bar{a}^2}\frac{\partial p'}{\partial r}+\bar{\rho}\frac{\partial u'}{\partial r}+u'\frac{\partial\bar{\rho}}{\partial r}+\frac{u'\bar{\rho}}{r}+\frac{\bar{\rho}\partial v'}{r\partial\theta}=0 \tag{A.10}$$

$$\frac{\partial u'}{\partial t}+\frac{\bar{v}\partial u'}{r\partial\theta}+\bar{u}\frac{\partial u'}{\partial r}+u'\frac{\partial\bar{u}}{\partial r}-\frac{2\bar{v}v'}{r}=-\frac{1}{\bar{\rho}}\frac{\partial p'}{\partial r}+\frac{p'}{\bar{\rho}^2\bar{a}^2}\frac{\partial\bar{p}}{\partial r} \tag{A.11}$$

$$\frac{\partial v}{\partial t} + \frac{\bar{v}\partial v'}{r\partial\theta} + \bar{u}\frac{\partial v'}{\partial r} + u'\frac{\partial \bar{v}}{\partial r} + \frac{u'\bar{v}}{r} + \frac{\bar{u}v'}{r} = -\frac{1}{\bar{\rho}r}\frac{\partial p'}{\partial\theta} \tag{A.12}$$

Assumed base flow, planar, incompressible, solid body rotation with no through flow:

$$\bar{w} = 0, \bar{v} = \Omega r, \bar{u} = 0 \tag{A.13}$$

This system of equations can then be solved as outlined in chapter 4.

Appendix B

Unsteady Velocity Response to Downstream Pressure Fluctuations as a Function of Reduced Frequency

The unsteady response of the flow in a duct to fluctuations in downstream pressure is derived here. This derivation follows closely to that developed in Greitzer et al. [4]. We begin by examining the flow in a one dimensional duct as shown in Fig. B-1.

In one dimension and assuming inviscid flow, the momentum equation is given by equation B.1.

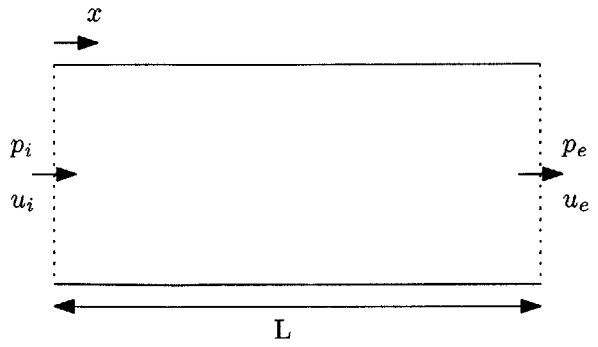

Figure B-1: 1-Dimensional duct flow schematic.

$$\frac{\partial u}{\partial t} + u\frac{\partial u}{\partial x} = -\frac{1}{\rho}\frac{\partial p}{\partial x} \tag{B.1}$$

The continuity equation is simply

$$\rho u A = Constant. \tag{B.2}$$

Since the duct is constant area and if we assume incompressible flow this simplifies to the statement that u is a constant throughout the duct. We can then integrate equation B.1 from the inlet to the exit.

$$L\frac{du}{dt} = -\left(\frac{p}{\rho} + \frac{u^2}{2}\right)_i^e \tag{B.3}$$

Now we apply a similar small disturbance flow analysis to that described in Appendix A. The flow is assumed to be a set of small disturbances superimposed upon a base flow.

$$p = \bar{p} + p' \tag{B.4}$$

$$u = \bar{u} + u' \tag{B.5}$$

substituting these into equation B.3 and neglecting second order terms (the product of disturbance quantities) gives:

$$L\frac{du}{dt} = \frac{\bar{P}_{ti} + P'_{te} - \bar{P}_{te} - P'_e}{\rho} - \bar{u}_e u' \tag{B.6}$$

The meanflow is assumed to be lossless so the inlet and exit total pressures are identical. We also assume that the inlet total pressure is held constant so $P'_{ti} = 0$. Equation B.6 can therefore be simplified to:

$$L\frac{du}{dt} = \frac{-P'_e}{\rho} - \bar{u}_e u' \tag{B.7}$$

If we assume the disturbances are in the form of normal modes, i.e.

$$p' = \hat{p}e^{-j\omega t} \tag{B.8}$$

and

$$u' = \hat{u}e^{-j\omega t} \tag{B.9}$$

we can substitute these into equation B.7 and solve for the velocity disturbance $\hat{u}$. Recognizing that the reduced frequency β is defined as $\frac{\omega L}{\bar{u}}$ the following equation describing the velocity response is obtained.

$$\frac{\hat{u}}{\frac{\hat{p}}{\rho\bar{u}}} = \frac{j\beta - 1}{1 + \beta^2} \tag{B.10}$$

This describes a semi-circle on the complex plane as shown in Fig. 3-15. The magnitude of the response is given by the magnitude of a vector from the origin to the circle.

Bibliography

[1] Electric power annual 2011. Technical report, Independent Statistics & Analysis, U.S. Department of Energy, Washington, D.C., January 2013.

[2] Go K Batchelor. Note on a class of solutions of the navier-stokes equations representing steady rotationally-symmetric flow. *The Quarterly Journal of Mechanics and Applied Mathematics*, 4(1):29–41, 1951.

[3] JW Daily and RE Nece. Chamber dimension effects on induced flow and frictional resistance of enclosed rotating disks. *Journal of Basic Engineering*, 82:217, 1960.

[4] Edward M Greitzer, Choon Sooi Tan, and Martin B Graf. *Internal flow: concepts and applications*, volume 3. Cambridge University Press, 2004.

[5] Nicholas J. Hills, John W. Chew, and Alan B. Turner. Computational and Mathematical Modeling of Turbine Rim Seal Ingestion. *Journal of Turbomachinery*, 124(2):306, 2002.

[6] Ralf Jakoby, T. Zierer, K. Lindblad, J. Larsson, Dachauer Strasse, Dieter E Bohn, Joachim Funcke, and Achim Decker. GT2004-53829 NUMERICAL SIMULATION OF THE UNSTEADY FLOW FIELD IN AN AXIAL GAS Vane hot gas Blade ingestion air Stator Rotor. *Proceedings Of The Asme Turbo Expo 2004*, pages 1–10, 2004.

[7] P Jenny, R Abhari, MG Rose, M Brettschneider, and J Gier. A low pressure turbine with profiled endwalls and purge flow operating with a pressure side bubble. *Journal of Turbomachinery*, 134(6):061038, 2012.

[8] G. M. Laskowski, R. S. Bunker, J. C. Bailey, G. Ledezma, S. Kapetanovic, G. M. Itzel, M. a. Sullivan, and T. R. Farrell. An Investigation of Turbine Wheelspace Cooling Flow Interactions With a Transonic Hot Gas PathPart II: CFD Simulations. *Journal of Turbomachinery*, 133(4):041020, 2011.

[9] J M Owen and U.P Phadke. An Investigation of Ingress for an Disk System With Radial- Clearance Seals. *Transactions of the ASME*, 105(January):8–12, 1983.

[10] J. Michael Owen. Prediction of Ingestion Through Turbine Rim SealsPart I: Rotationally Induced Ingress. *Journal of Turbomachinery*, 133(3):031005, 2011.

[11] J. Michael Owen. Prediction of Ingestion Through Turbine Rim SealsPart II: Externally Induced and Combined Ingress. *Journal of Turbomachinery*, 133(3):031006, 2011.

[12] J. Michael Owen, Kunyuan Zhou, Oliver Pountney, Mike Wilson, and Gary Lock. Prediction of Ingress Through Turbine Rim SealsPart I: Externally Induced Ingress. *Journal of Turbomachinery*, 134(3):031012, 2012.

[13] K Stewartson. On the flow between two rotating coaxial disks. *Proc. Camb. Phil. Soc*, (July):333–341, 1953.

[14] Metodi Zlatinov. Secondary air interaction with main flow in axial turbines. Master's thesis, Massachusetts Institute of Technology, June 2011.